

## Crystalline and amorphous ices

V. FUENTES-LANDETE, C. MITTERDORFER, P. H. HANDLE, G. N. RUIZ,  
J. BERNARD, A. BOGDAN, M. SEIDL, K. AMANN-WINKEL, J. STERN,  
S. FUHRMANN and T. LOERTING(\*)

*Institute of Physical Chemistry, University of Innsbruck  
Innrain 80-82, A-6020 Innsbruck, Austria*

**Summary.** — Water is one of the most abundant molecules on Earth, of paramount importance to our daily lives and is of great relevance in astrophysics. Nevertheless its physical and chemical properties, which are often called anomalous, are not fully understood by now. Investigations in recent decades have shown that water exists in many crystalline forms — a phenomenon known as “polymorphism” — and in three amorphous forms — a phenomenon known as “polyamorphism”. In this article we review the crystalline ice phases and outline possibilities for future experimental discoveries of ice polymorphs. We then provide an overview about the current knowledge on polyamorphism and finally go into more detail about the question whether or not the amorphous ices are linked by glass-to-liquid transitions to deeply supercooled liquids, which has been a major focus in our research group over the last years.

---

(\*) E-mail: [thomas.loerting@uibk.ac.at](mailto:thomas.loerting@uibk.ac.at)

## 1. – Introduction

Water is ubiquitous and anomalous. Our planet is called the “blue planet” because water covers about 70% of its surface, and water is regarded as the “molecule of life” because it is vital to all known forms of life. Despite this key role, an understanding of many of its properties has remained elusive. In a rather narrow range of temperature and pressure water appears in all three common states of matter: vapour, solid and liquid. In the phase diagram of water the liquid and the vapour phase are separated by a coexistence line, which emerges from the vapour-liquid-solid triple point at 273.16 K (0.01 °C) and 612 Pa (6.12 mbar) and ends in the vapour-liquid critical point at 647.10 K (373.95 °C) and 22.1 MPa (221 bar) [1]. Above this (first) critical point water becomes supercritical. The occurrence of the vapour-liquid-solid triple point, the vapour-liquid critical point and the supercritical state are features found commonly in one-component systems, and hence do not make water anomalous. While it is clear that there is only one vapour phase (which can be continuously tuned in terms of its density), it is not clear how many condensed phases of water can be distinguished. In the solid state the concept of polymorphism has been established [2] and is regarded as one of water’s anomalies. It is an important concept in one-component systems, recognized about 200 years ago for the examples of carbonate, phosphate and arsenate salts [3,4]. In the case of water an anomalously wide variety of crystalline phases has been recognized. Some comprehensive reviews have been published in the past decade on these topics [5-8]. Water is also anomalous in that it shows three different amorphous states, which may be linked to three equilibrium liquids. Water was the first example for which such “polyamorphism” was discovered in 1984, and hence research on “polyamorphism” has still not reached a mature stage. Recently, the possibility of glass-to-liquid transitions in these amorphous ices was investigated, which would provide a link between the amorphous states and the supercooled liquids. In this article we first focus on the crystalline phases of ices and open questions related to them and then go on to the amorphous phases, their preparation and the characterization, the possibility of glass-to-liquid transitions connecting them to deeply supercooled liquids and also emphasize open questions related to amorphous ices.

## 2. – Crystalline ices

**2.1. *Stable phases, metastable phases and the melting line.*** – The special course of water’s melting line is most rarely found for other one-component systems (see fig. 1).

First of all, the melting line of solid water (ice), which also emerges from the vapour-liquid-solid triple point, is negatively sloped. Therefore, the process of pressure-induced melting may take place. An ice cube kept in the freezer at 255 K (–18 °C) will melt if the external pressure exceeds  $\sim 200$  MPa. Secondly, the melting line suddenly becomes positively sloped at 251 K and  $\sim 210$  MPa, and from that point on the process of pressure-induced crystallization may take place. A pressure-molten ice cube kept in the freezer at 255 K will refreeze again if the external pressure exceeds  $\sim 300$  MPa. It will not freeze to common hexagonal ice (ice  $I_h$ ), but to a different polymorph, namely ice III [9, 10].

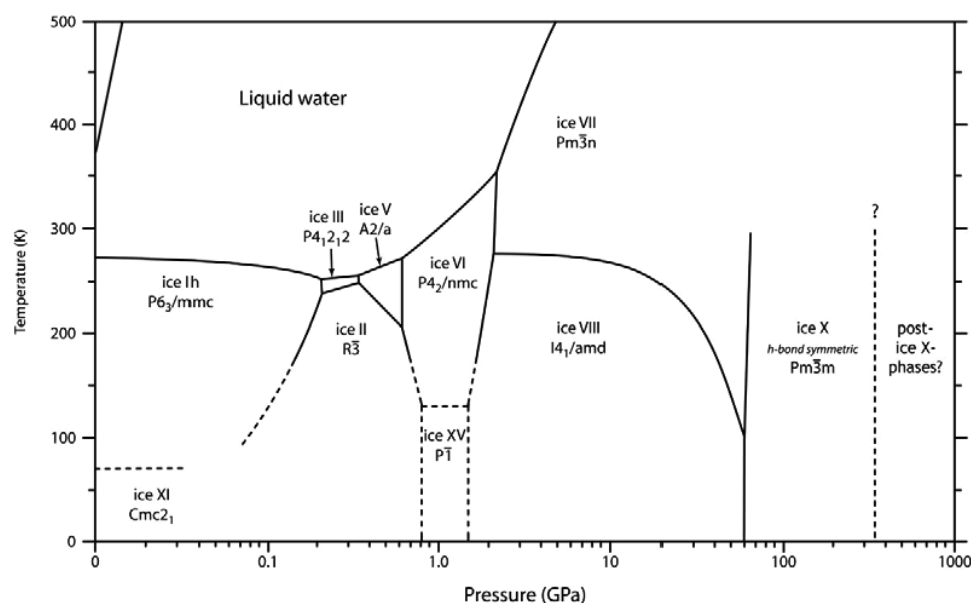


Fig. 1. – Phase diagram of water’s stable phases at positive pressure up to 1000 GPa (logarithmic axis) and temperature up to 500 K (linear axis). The regions of stability for ten ice polymorphs (Roman numerals), their space groups, the liquid and the gas-phase (top left corner) are shown. At the high-pressure end predicted post-ice X phases are indicated. Metastable polymorphs and amorphous phases are not evident in this diagram. Adapted from the webpage by Dominic Fortes (accessed on October 25, 2013: [http://www.homepages.ucl.ac.uk/~ucfbanf/research/water\\_ice.htm](http://www.homepages.ucl.ac.uk/~ucfbanf/research/water_ice.htm)).

An ice cube kept at 263 K ( $-10\text{ }^{\circ}\text{C}$ ) will melt earlier (above  $\sim 100\text{ MPa}$ ) and refreeze later (above  $\sim 450\text{ MPa}$ ), yet to another polymorph, namely ice V [11]. Compression of liquid water at ambient temperature to beyond  $\sim 900\text{ MPa}$  will result in the crystallization of ice VI [12]. Finally, when compressing hot steam kept isothermally at 800 K, ice VII [13-15] would be expected to crystallize from the supercritical state above  $\sim 20\text{--}40\text{ GPa}$  in a gedankenexperiment. Above 1000 K and above 50 GPa, yet another phase is accessible regarded as either ice X [16] or as a superionic state, in which the protons in ice VII are dynamically disordered [17]. In total, five solid-solid-liquid triple points have been identified along water’s melting line, at which its slope changes suddenly, and six different phases of ice are associated with them (ice  $I_h$ , ice III, ice V, ice VI, ice VII, ice X/superionic ice). The melting line of water is reasonably well understood, and so it seems clear that there are six different ice phases associated with it.

In addition, also solid-solid-solid triple points are known at which three solid polymorphs coexist. In particular, ice II [18-22], ice VIII [23-37], ice XI [33, 34, 37-42], ice XIII [43-48], ice XIV [45, 49, 50] and ice XV [24, 37, 51-53] can exist in thermodynamic equilibrium exclusively with other polymorphs of ice. Solid-solid transitions involved

in obtaining phases not in equilibrium with liquid water may either involve rearrangement of the lattice of oxygen atoms and be driven by changes in density, *e.g.*, when pressurizing ice I<sub>h</sub> to ice II [54]. Alternatively proton-ordering transitions to a proton-ordered phase may be driven by entropy, *e.g.*, when cooling ice III to proton-ordered ice IX [37, 43, 44, 55-60]. The variety of phases of ice encountered in particular in the pressure range up to 2 GPa (see fig. 1) originates not only from the phases mentioned so far, but also from phases, which are presumed to be metastable. Such phases do not appear in the phase diagram of stable phases (see fig. 1), but may occur due to the fact that the thermodynamically most stable phase cannot be accessed easily because of kinetic or geometric constraints. In particular, ice IV [61-65] or ice XII [64-74] may crystallize from the pressurized liquid or amorphous solid state (rather than the stable phases ice V and ice VI) as metastable polymorphs. Cubic ice (ice I<sub>c</sub>) [75] may as well crystallize from ambient water under special circumstances [76] or may be obtained by heating high-pressure polymorphs or amorphous ice at ambient pressure [77-79]. In terms of free energies these metastable phases may be very close to the stable phases. In fact, it is very challenging to reproduce the order of stability found experimentally in simulations. By contrast to the experimental findings, some models describe cubic ice (ice I<sub>c</sub>) to be more stable than hexagonal ice (ice I<sub>h</sub>), ice IX to be more stable than ice II and ice XII and XIV to be more stable than ice V [80], or ice II to be stable over a wide range of pressure and temperature where hexagonal ice, ice III and ice V are found to be stable in experiment [81]. The preparation of these metastable phases can be described as an “art” rather than as a “science”. For instance, ice IV has originally been described as “a will-o’-the-wisp, a tentative, ghostly form of ice” [61, 62]. Selected organic nucleating agents were added to pressurized liquid water in order to specifically nucleate certain high-pressure forms of ice such as ice IV [82], and these nucleation experiments successfully produced the desired polymorph possibly in one out of ten attempts. Also ice XII belongs to the metastable polymorphs of ice, which may nucleate from pressurized liquid water. In addition to nucleation from the liquid also crystallization from high-density amorphous ice at low temperature was found to produce ice XII [64, 68-74, 83, 84]. Ice XII differs in terms of the oxygen lattice from all other known ice phases, and its discovery in 1998 represents the latest discovery of a novel way of arranging water oxygen atoms in a lattice of water molecules [66]. The latest discovery of a polymorph of ice differing in terms of the proton lattice, namely ice XV, was reported in 2009 [53]. On average, a new ice polymorph was discovered every six years in the last century. New ice polymorphs may be discovered in the future. Traditionally, Roman numerals are used for naming ice phases. The numbering follows the chronological order of their discovery, *i.e.*, the next ice phase to be discovered will be named ice XVI. Ices XIII, XIV and XV were discovered within the last five years and represent proton-ordered variants of previously known ice polymorphs. Ice XVI may well be another proton-ordered variant of a known polymorph. However, it may also be a new metastable form of ice easily accessible in the pressure range up to 2 GPa, it may be a form stable at extremely high pressure on the order of 1000 GPa or it may be a form stable at negative pressure, *e.g.*, -500 MPa. Before discussing these extremes of positive and negative pressure, we devote a few words to

the two ice polymorphs accessible without the use of high-pressure equipment at ambient pressure, which are somewhat surprisingly both called ice I.

**2.2. Ice I: cubic ice and hexagonal ice.** – Cubic ice (ice  $I_c$ ) and hexagonal ice (ice  $I_h$ ) are very similar, show the same interatomic distances and approximately the same density of  $0.92\text{ g/cm}^3$  at ambient pressure [85]. There is particular interest in these two because they represent the low-density forms of ice existing at ambient pressure. Hexagonal ice is ubiquitous and occurs in the form of snowflakes, icicles, ice, hail, etc., whereas cubic ice may appear occasionally in clouds [76, 86, 87]. They appear to be identical when studying them using a method sensitive to the local, short-range molecular environment. For instance, vibrational spectroscopy mainly probes local oscillations of atom groups. The Raman spectrum of cubic ice is identical to the Raman spectrum of hexagonal ice. Mid-infrared spectroscopy is also not able to distinguish between the two and consequently both of these ices are called ice I. The difference between them is found when comparing the long-range order of the hexagonal rings building the crystal structures. Whereas cubic ice shows the stacking sequence ABCABCABC forming a face-centered cubic lattice, hexagonal ice shows the stacking sequence ABABAB forming a hexagonal lattice. At ambient pressure hexagonal ice is only slightly more stable than cubic ice [88-90]. Only methods sensitive to long-range order such as neutron or X-ray diffraction clearly show the structural difference between the two [91]. Using the definition of polytypism “for structural modifications, each of which can be regarded as built up by stacking layers of (nearly) identical structure and composition differing only in their stacking sequence” [92], hexagonal ice and cubic ice are regarded as two polytypes, which belong to two different space groups ( $P63/mmc$  vs.  $Fd3m$ ) [91, 93, 94]. This certainly provides the basis for identifying and counting them as two distinct ice polymorphs. However, by contrast to hexagonal ice, cubic ice cannot be obtained in the form of a large  $Fd3m$  single crystal. Cubic ice can be obtained only in the form of very small crystallites, and it always contains more or less hexagonal stacking faults. Hexagonal stacking faults can be clearly identified in diffraction experiments [91, 95, 96].

In fig. 2 powder X-ray diffractograms for hexagonal ice and cubic ice are depicted along with the theoretical models for the diffraction patterns. The hexagonal (100) reflection is generally observed in samples of cubic ice, as seen in the diffractogram depicted in fig. 2 (second from top). Its intensity, however, changes with changing preparation history as seen in fig. 2 (third diffractogram from top). Hansen *et al.* have defined a “cubicity index” for describing different degrees of stacking faults observed in diffraction patterns [98, 99]. Similarly, hexagonal ice may contain cubic stacking faults, and highly stacking-faulty ice I may be regarded with equal justification either as “cubic ice with hexagonal deformation stacking-faults” or as “hexagonal ice with cubic deformation stacking-faults”. The transition from cubic ice to hexagonal ice does not take place at a well-defined temperature, but depends on the preparation history, *i.e.*, “cubicity”. Its onset temperature varies by more than 30 K in various calorimetry experiments [88, 89]. A slow change of stacking sequence may be observed even at 190 K, whereas a faster, collective transition to hexagonal ice typically occurs around 220 K [88]. This is explained

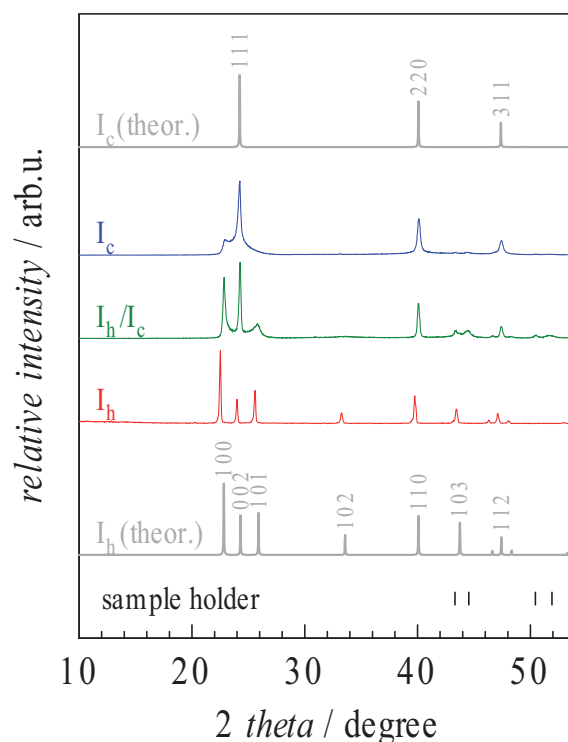


Fig. 2. – Calculated (labelled “theor.”) and measured powder X-ray diffractograms for cubic ice  $I_c$  and hexagonal ice  $I_h$ , and a sample, which cannot be clearly categorized as either cubic or hexagonal ice. Miller indices are indicated in the case of calculated diffractograms. Measurements were done in  $\Theta$ - $\Theta$  arrangement on a Siemens D5000 diffractometer (using  $\text{Cu-K}\alpha_1$ -rays) at  $\sim 85$  K in the case of diffractograms labelled  $I_c$  and  $I_c/I_h$  and at  $\sim 250$  K in the case of the diffractogram labelled  $I_h$ . Calculations were done using the published crystal structures of ice  $I_h$  [94] and ice  $I_c$  [75]. The disagreement between the calculated and observed powder pattern for cubic ice  $I_c$  is explained in terms of hexagonal stacking faults, also known as deformation faults [97].

in the sense that a highly stacking faulty cubic ice would transform at lower temperature, whereas cubic ice largely free of hexagonal stacking faults would transform at higher temperature. A single crystal of cubic ice, if it was experimentally accessible, may transform to hexagonal ice even close to the melting point. The key question related to counting ice polymorphs, therefore, seems to be whether or not the experimentally observable “cubic ice” should be regarded as a polymorph different from hexagonal ice or whether it should be regarded as hexagonal ice containing a large number of cubic stacking faults. The common practice in the scientific community is to call both of them ice I, but to regard them as two distinct polytypes. Polytypism is a special type of polymorphism characterized in that two polytypes differ only in the stacking of identical, two-dimensional sheets or layers.

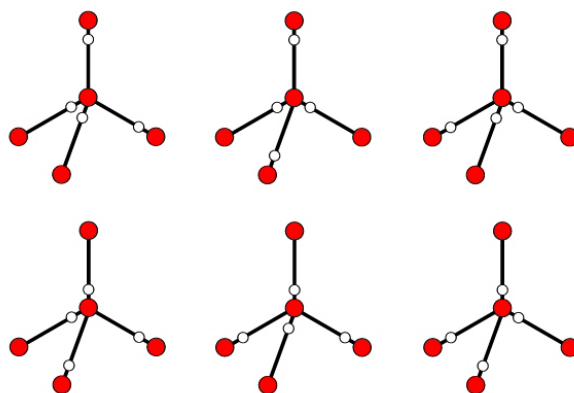


Fig. 3. – Six possible molecular orientations of a central water molecule in the Walrafen-pentamer, *i.e.*, a central oxygen atom (red) tetrahedrally surrounded by four oxygen atoms (red). These six configurations, but no others, can be obtained by distributing four protons (white) in accordance with the Bernal-Fowler rules. Each proton may sit on one of two possible positions along the line connecting two oxygen atoms (black lines), and there must be one proton sitting on each line.

**2.3. Proton order-disorder transitions.** – Ice polymorphs often come in pairs. Currently, the six pairs I<sub>h</sub>-XI [33, 34, 37-42], III-IX [37, 43, 44, 55-60], V-XIII [43-48, 100, 101], VI-XV [24, 37, 51-53], VII-VIII [23-37] and XII-XIV [45, 49, 50, 100, 101] are known. These pairs of crystalline ices are characterized in that the polymorph mentioned first is a proton-disordered form, which occurs at high temperature, whereas the polymorph mentioned second is a proton-ordered form, which occurs at low temperature. Both ices, however, are characterized by a topologically identical lattice of oxygen atoms.

When considering a Walrafen-pentamer of water molecules (see fig. 3), there are six different possibilities of how to arrange hydrogen atoms in accordance with the Bernal-Fowler rules [102]. In fully proton-disordered ices all these configurations are populated with equal probability when averaging over space and time. That is, six orientations of a given water molecule are possible at any time, and these orientations may be converted into each other by rearrangement of the protons and/or rotation of water molecules. This rearrangement is alleviated by mobile point defects such as Bjerrum L-defects (no proton between two oxygen neighbours), which migrate through the crystal. While a proton-ordered configuration is more favourable in terms of enthalpy, the proton-disordered configuration is more favourable in terms of entropy. When the temperature is lowered the orientation of water molecules tends to become more ordered. However, the mobility of intrinsic point defects may be too low at low temperature, resulting in an immobilized proton-disordered form of ice rather than the more favourable proton-ordered form. This is observed, *e.g.*, when cooling proton-disordered hexagonal ice to 10 K. The number of point defects, in particular of Bjerrum L- and Bjerrum D-defects (no or two protons between two oxygen neighbours) and ionic defects (H<sub>3</sub>O<sup>+</sup> or OH<sup>-</sup> ions) can be increased, though, by doping the ice lattice with a small amount of small molecules such as HF,

HCl, KOH or  $\text{NH}_3$ . These molecules are incorporated as substitutional point defects directly into the ice lattice by replacing water molecules [1]. Typically, concentrations on the order of  $10^{-4}$ – $10^{-2}$  M are used, corresponding to molar ratios of 1:500000–1:5000, respectively. In the presence of these extrinsic defects the kinetically hindered ordering of protons may be facilitated. Using a suitable temperature protocol and a suitable catalyst, namely KOH, proton ordering in ice  $I_h$  takes place at temperatures slightly below 72 K after weeks [38, 39]. The understanding of the mechanism underlying this increase in mobility is far from complete. For instance, in case of the ordering transition from ice V to ice XIII, HCl (producing Bjerrum L-defects) is effective, whereas KOH (producing Bjerrum L-defects and ionic  $\text{OH}^-$  defects) is ineffective. On the other hand, in case of the ordering transition from ice  $I_h$  to ice XI, HCl is effective. An understanding of the proton-ordering mechanism and how to facilitate it would be highly desirable, in particular because proton-ordered cubic ice  $I_c$  [103, 104], proton-ordered ice IV and proton-disordered ice II have not been prepared in laboratory experiments yet.

Furthermore, we want to emphasize that there is not only one possibility how the protons can order. In fact, there are numerous proton-ordered structures related to the same proton-disordered polymorph. 75 years ago Pauling had regarded all proton-ordered structures obtainable by simply permuting protons as degenerate [105]. It is clear now, though, that there are subtle differences in enthalpy, and also in the lattice parameters and density. One issue, which may be discussed controversially, is the issue of incomplete transformation. For instance, partial ordering of protons has been observed in ice V [43, 44], but the crystal structure of the completely ordered polymorph ice XIII could be refined only later [45]. In case of the ordered form of ice XII an incompletely ordered polymorph containing residual disorder was refined to the crystal structure of ice XIV [45]. This has prompted theoreticians to propose that differently ordered variants of ice XIV may exist and be at the origin of the residual disorder [50]. The data extracted from neutron scattering experiments indicate that four out of eight protons in the unit cell are not fully ordered [45]. This was regarded as residual disorder at first [45], but explained in subsequent theoretical work by the simultaneous presence of two or three different proton-ordered configurations (ice XIV, ice XIV' and ice XIV''), which differ slightly in terms of energy per molecule (by less than 1 kJ/mol) and lattice parameters (by  $\sim 0.5\%$ ). All of them belong to the same space group  $P2_12_12_1$ , though. This space group is necessarily a subgroup of the space group, to which the parent proton-disordered polymorph ice XII belongs ( $I42d$ ). Even though the three types of ice XIV belong to the same space group, they differ in terms of the crystallographic lattice. That is, there are a number of possibilities how protons may order, which result in configurations of similar enthalpy. One of these configurations corresponds to the experimentally verified polymorph, and the others might be detected in future laboratory experiments.

**2.4. Ice X and post-ice X phases.** – All crystalline ices are characterized by well-defined water molecules bonded by relatively weak hydrogen bonds. Ice X, predicted in 1972 by Holzapfel [106], is the exception. Water molecules are no longer uniquely defined in ice X, because H atoms occupy the position exactly halfway between two O-atoms (“halfway

position”). Ice X has, therefore, also been called “symmetric ice” [107, 108] and can be regarded as an atomic crystal with two-thirds H-atoms and one-third O-atoms [109]. About a decade later changes in the Raman spectrum of ice VII in the pressure range  $\sim 35\text{--}50$  GPa were interpreted by Hirsch and Holzapfel [110, 111] to be consistent with H-bond symmetrisation and ice X formation. Also anomalies in the behaviour of the longitudinal sound velocity in ice VII found by Polian *et al.* using Brillouin scattering experiments are consistent with a phase transition in this pressure range, possibly to ice X [107, 108]. Changes in infrared active modes are consistent with the idea of H-bond symmetrisation [32, 112–114]. The “halfway position” may either be a result of statistically averaging H-atoms being delocalized in a shallow double-well potential or of the H-atoms being localized in a single-well potential [115]. While the former is referred to as “disordered ice X” the latter is referred to as “ordered ice X”. Pruzan *et al.* have argued on the basis of Raman and X-ray diffraction data that the statistically averaged, disordered form is encountered [116]. This form is, however, not much different from ice VII with a strong dynamic disorder of protons along O...O directions (see fig. 2 in ref. [109]). Both ice VII and ice X show a body-centered cubic (bcc) sublattice of oxygen atoms [117]. The main difference being that in ice VII the proton distribution has two maxima along O...O directions, whereas in ice X the proton distribution has only one maximum in the “halfway position” as a result of the quantum effect zero-point motion [118]. Goncharov *et al.*, on the other hand, interpret their results from high-pressure Raman and infrared studies on the basis of a static, ordered ice X, which forms from ice VII above  $\sim 60$  GPa [119, 120] of the cuprite, single-well type. This ordered ice X is thought to be stable up to ultrahigh pressure of at least 200 GPa. The debate about the mechanism of the transition from ice VII to ice X was recently made richer by a neutron diffraction study of D<sub>2</sub>O-ice VII [121]. In this study, the authors claim that the disordering mechanism in ice VII starts at about 13 GPa by localizing a protonic species at the octahedral interstitial sites of the oxygen sublattice rather than at the lines connecting oxygen atoms [121]. Above 13 GPa anomalous behaviour was noticed in spectroscopic work [121], and also the ice VII/ice VIII phase boundary starts to deviate from being parallel to the pressure axis (see fig. 1).

At  $> 200$  GPa a transition to a post-ice X phase of orthorhombic structure (*Pbcm*) has been predicted [122]. A dynamic instability in ice X is thought to be underlying the transition ice X  $\rightarrow$  *Pbcm* [123, 124]. Another option was suggested by Demontis *et al.*, who predict a transition from the body-centered cubic (bcc) cuprite structure in ice X to a face-centered cubic (fcc) antiferite structure (*Pm-3m*). Originally they predicted the transition to occur at  $\sim 100$  GPa [125]. However, in view of diamond anvil studies not indicating any kind of transition close to 100 GPa, they refined the transition pressure to  $\sim 330$  GPa [126]. Very recently Miltzer and Wilson have predicted that at 760 GPa a transition to *Pbca*, and at 1550 GPa a transition to *Cmcm* takes place [127]. Their predicted phases are depicted in fig. 4.

The *Pbca* phase is an insulator and consists of an interpenetrating network, just like ice VII, VIII and X. The *Cmcm* phase, however, is metallic and consists of corrugated sheets and the H-atoms no longer occupy tetrahedral sites between nearest O-atoms, but

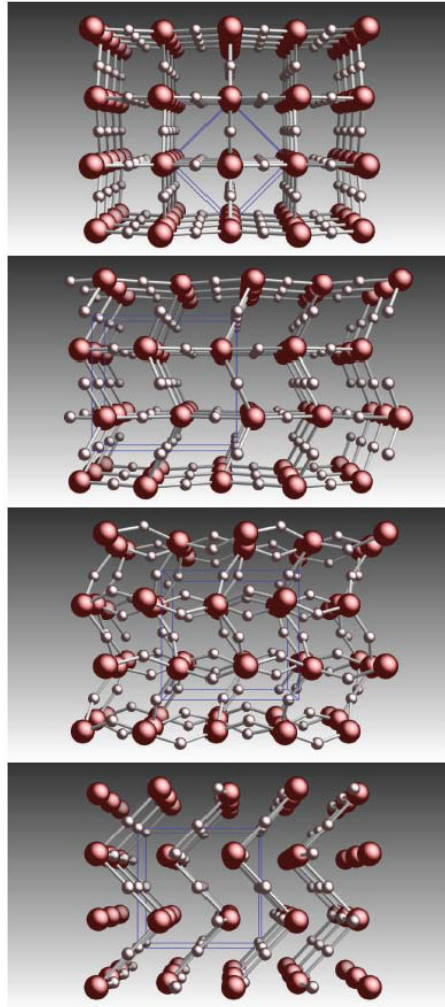


Fig. 4. – Structures of the ice X phase (top), predicted *Pbcm* phase (2nd from top), predicted *Pbca* (3rd from top) and predicted *Cmcmm* (bottom) phases. The large and small spheres denote the O and H atoms, respectively, while the thin blue lines denote the unit cells. The ice X to *Pbcm* transition is a displacement of atomic layers. In *Pbca*, the H atoms are squeezed out of midpoint between nearest O atoms. In *Cmcmm*, the H atoms occupy mid-points between next-nearest O atoms. Reproduced from ref. [127].

octahedral, midpoint positions between next-nearest O-atoms. When considering also differences in zero-point energy, the orthorhombic *Pnma* phase (related to the *Cmcmm* phase by a slight Peierls lattice distortion) appears as a stable phase in the range of 1250–1550 GPa prior to the transformation to the metallic *Cmcmm* phase. Such a metallic phase may be accessible only at very high temperature, *e.g.*, at  $T > 7000$  K, and a superionic

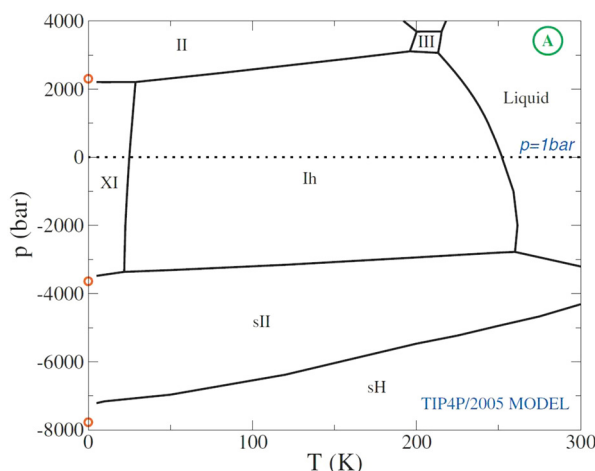


Fig. 5. – Phase diagram of water as predicted by using the TIP4P/2005 potential. At positive pressure the known low-density polymorphs ice  $I_h$  and ice XI and the known high-pressure polymorphs ice II and ice III are predicted to be stable in agreement with experimental observations. On the negative pressure side, novel polymorphs of even lower density (denoted sII and sH) are predicted to be stable. Other open networks of cage-like structures such as ice  $i'$  and sI are predicted to be similar in energy to sII and sH. The structures sI, sII and sH are depicted in fig. 6. For simulation details please refer to ref. [135]. Reproduced from ref. [135].

phase is expected below that temperature [128]. To date there is no experimental evidence for any of these predicted phases, but one or the other might well be detectable in the future when new experimental techniques become available or the capabilities of existing techniques are exploited.

**2.5. Negative pressure.** – If one wanted to observe freezing of liquid water at ambient temperature, negative pressure on the order of  $-200$  MPa would be required. However, liquid water at ambient temperature cannot sustain such a tension [129]. Cavitation, *i.e.*, nucleation and growth of a bubble, is observed around  $-20$  MPa [130, 131], and in other experiments around  $-100$  MPa [132, 133]. The existence of ice I crystals at  $+6.5^\circ\text{C}$  has been reported in some microscopic inclusions in minerals [134]. No solid phase other than ice I has been observed at negative pressure so far. However, calculations indicate that other phases may be thermodynamically more stable than hexagonal ice. In particular, open cage-like structures (“nanocages”) have been predicted to be stable (fig. 5) [135].

These cages resemble the cages observed in natural clathrate hydrates [136]. While the cavities in clathrate hydrates are stabilized by van der Waals interactions with guest molecules (*e.g.*, methane), the cavities predicted at negative pressure are empty. The three most common types of clathrate hydrates belong to three different types of structures built from differently sized cages. They are called cubic structure I (sI), cubic structure II (sII) and hexagonal structure (sH). Figure 6 shows the construction princi-

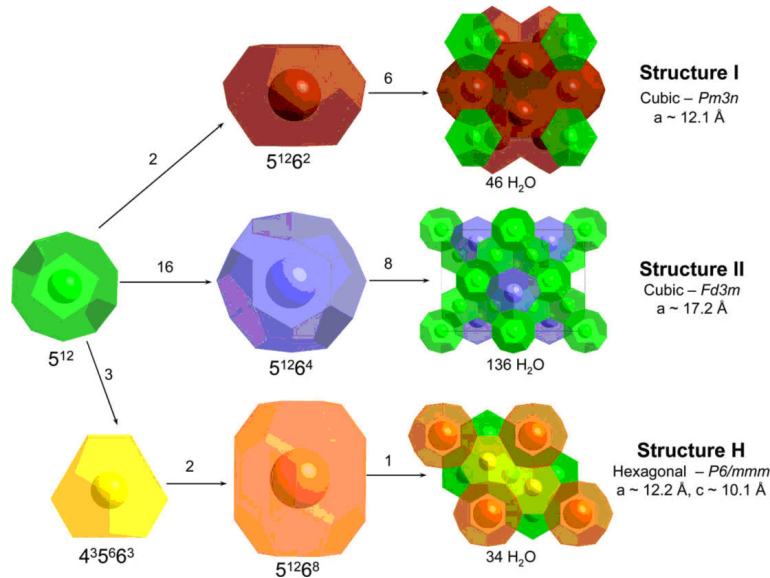


Fig. 6. – Building principle of the common clathrate hydrate structure I (sI), structure II (sII) and structure H (sH). All structures are built from differently sized “nanocages”. For example, the notation  $5^{12}6^2$  refers to a nanocage consisting of twelve water-pentagons and two water-hexagons. The numbers on the arrows refer to the numbers of such nanocages building the unit cell of the individual structures. For instance, the unit cell of sI includes two  $5^{12}$  nanocages and six  $5^{12}6^2$  nanocages. The total number of water molecules in the unit cell, the crystal system, the space group and the lattice constants  $a$  and  $c$  are indicated. Reproduced from ref. [137].

ple of these cage structures as deduced from studies on clathrate hydrates [137]. These structures contain differently sized cages built from a differing number of four-, five- and six-membered rings of water molecules (fig. 6). The same types of cages are predicted to be stable crystals at negative pressure even in the absence of guest molecules. For instance, the TIP4P/2005 model predicts the sII structure to be stable at negative pressure on the order of  $-400 \text{ MPa}$  and the sH structure to be stable at negative pressure on the order of  $-700 \text{ MPa}$  (fig. 5) whilst the mW-water model predicts the sII structure to be stable even at a pressure lower than  $-130 \text{ MPa}$  [138]. The sI phase is metastable by only a slight difference in chemical potential in the sII region of stability [135]. Other crystalline phases, which are necessarily of lower density than hexagonal ice [139], have been predicted in other simulations, *e.g.*, ice *i* and ice *i'* [140]. Using the TIP5P model it is predicted that hexagonal ice under tension would transform first to ice *i'*. At higher tension the latter would transform to sII and finally at the highest tension considered in the simulations of  $-1 \text{ GPa}$  to sH. For some water models such as TIP4P/2005 it has been shown that they fare reasonably well in predicting the phase diagram of water [141], and so it seems justified to expect that one or the other low-density phase may be accessible in future when doing experiments on stretched ice or stretched water.

**2'6. Summary: crystalline ices.** – So, currently techniques exist to prepare crystalline ices I–XV in the laboratory. In ice I the distinction between hexagonal ice (ice  $I_h$ ) and cubic ice (ice  $I_c$ ) is commonly made, even though a “pure” single crystal of ice  $I_c$  has never been observed. When still counting both ice  $I_c$  and ice  $I_h$  as distinct polytypes of ice, then 16 crystalline polymorphs of ice have been obtained in laboratory experiments so far. These 16 phases are characterized by well-defined crystal structures. The crystal structures are known to a high precision, often also as a function of temperature and/or pressure [85]. Barely anyone doubts the space groups and lattice positions of water molecules in these crystal structures.

Candidates for future discovery of ice polymorphs are proton-ordered variants related to known proton-disordered polymorphs. Also polymorphs differing in terms of oxygen positions may be discovered in future experiments. In particular the intermediate pressure range 0.2–2.0 GPa, which is very rich in different stable and metastable ice polymorphs, may reveal one or the other new polymorph despite more than 100 years of its exploration. Other pressure regimes, which have not been explored very much in past experiments such as the domain of negative pressure (“stretched ice”) and of extremely high pressure on the order of  $> 200$  GPa might also contain novel ice polymorphs. Open cage-like structures identical to some known clathrate hydrate structures, but free of (non-water) guest molecules, have been predicted to be stable at negative pressure [135, 138]. On the other hand a range of so-called post ice X phases has been predicted to be stable at extremes of high pressure, which can be reached in laboratory experiments only with difficulties [142]. Even if such pressure can be reached, it will be an experimental challenge to characterize the material in these environments. In particular, solving the crystal structure will be a major challenge. That is, new ice polymorphs will likely be discovered in the future when new experimental methods become available or when some clever experiments are done using existing technologies.

### 3. – Amorphous ices

**3'1. Motivation.** – Amorphous ices do not appear in the phase diagram of stable phases (see fig. 1) because of their metastable nature. In spite of this, the most abundant form of appearance of solid water in the universe is as amorphous ice [143]. The physico-chemical properties of interstellar dust grains in dense molecular clouds, and thus the process of star formation, and comets are governed by the properties of amorphous ice. Earth is one of the exceptions in the universe, with practically all solid water appearing as hexagonal ice, because temperatures on Earth exceed 150 K, above which amorphous ices typically crystallize. There may be some rare exceptions in clouds, which may occasionally also host cubic ice [76, 87] or in high-altitude, noctilucent clouds even amorphous water [144]. Furthermore, cold subducting slabs in the interior may host high-pressure forms of crystalline ice [145].

The motivation for studying amorphous, solid forms of water, however, very often originates in the desire to understand why liquid water is so special, of vital importance for life [146] and very different from other, so-called simple liquids. The outstanding

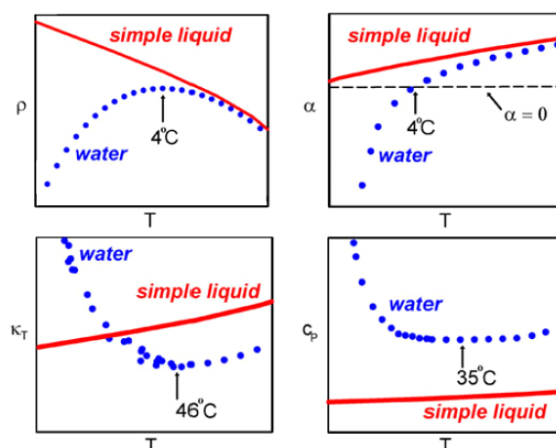


Fig. 7. – Isobaric temperature dependence of the density, the thermal expansion coefficient, the isothermal compressibility and the isobaric heat capacity for water (blue dotted line) and for a simple liquid (red line). Reproduced from ref. [146].

nature of liquid water, especially in the cold and supercooled state is demonstrated in fig. 7 [146]. This includes the well-known density maximum at 4 °C, and a strong increase of both the isothermal compressibility  $\kappa_T$  and the isobaric heat capacity  $C_p$  upon cooling. As of Nov. 25, 2014, in total 72 anomalies have been collected by Prof. Martin Chaplin on the webpage <http://www1.lsbu.ac.uk/water/anmlies.html>, which are grouped as density, thermodynamic, material, physical and phase anomalies. The latter category includes the rich polymorphism described above, but also polyamorphism.

In fact, water was the first example for which polyamorphism (amorphous polymorphism) was discovered in pioneering studies by Osamu Mishima *et al.* [147]. Mishima succeeded in preparing high- (HDA) and low-density amorphous ice (LDA) starting from hexagonal ice (see sect. 3'2) [147]. The idea behind these studies is a thermodynamically continuous link between the amorphous ices and supercooled equilibrium liquids, called high-density liquid (HDL) and low-density liquid (LDL), respectively [147]. The existence of such a link is highly debated, though, and requires to study whether amorphous ices experience glass-to-liquid transitions upon heating.

In the last decade the study of amorphous ices has seen significant progress, which we cover here. A more detailed review about research on amorphous ices, including molecular simulations (which are omitted here), can be found in several places [146, 148-151]. To set this review apart from the recent others we here focus the discussion especially on (calorimetric) studies about the glass transition in the several forms of amorphous ice.

**3'2. Formation/preparation.** – Preparation routes for amorphous ices are summarized in fig. 8. Amorphous solid water (for short ASW) was produced for the first time in the laboratory by Burton and Oliver in 1935 [152] using the technique of water va-

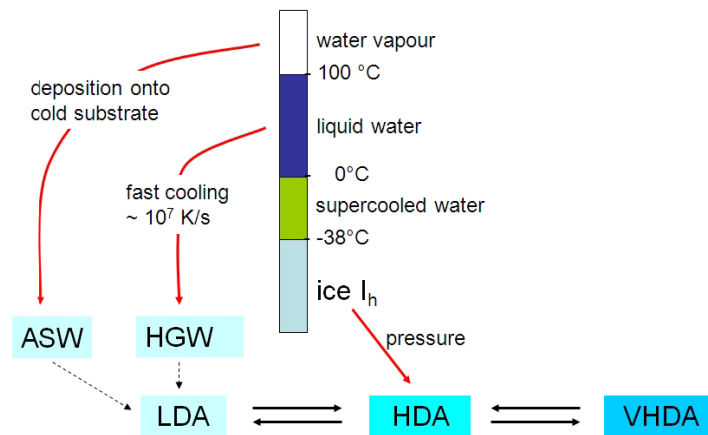


Fig. 8. – Summary of preparation routes for amorphous ices in the laboratory. ASW: amorphous solid water, HGW: hyperquenched glassy water, LDA/HDA/VHDA: low-/ high-/ very high-density amorphous ice. Red arrows indicate sharp transitions, black dashed arrows indicate slow annealing.

por deposition onto a cold copper rod [152], where deposition below 130 K leads to an amorphous solid. ASW is of astrophysical relevance and supposed to occur in comets, in the satellites of the outer planets as well as on the interstellar dust [153]. Similar to the lab preparation procedure, ASW accretes onto dust particles in the cold regions of dense interstellar clouds, especially in shocked molecular clouds [154]. Alternatively, ASW may form by chemical reactions between H, O and OH, especially in cold dark-star forming clouds. ASW plays a key role in promoting chemical reactions, acting as a reservoir trapping volatile gases, and potentially is pivotal in the earliest stages of planet building. Generally the deposition conditions (substrate temperature, incidence angle of water molecules, etc.) strongly influence the properties of the water vapor deposit [155]. Under certain deposition conditions ASW is a highly microporous solid, whereas it is a compact solid under different deposition conditions [155]. Specific surface areas of up to 2000 m<sup>2</sup>/g were reported, which are reduced to less than 1 m<sup>2</sup>/g after collapse of the micropores [156]. During this collapse process, volatile molecules adsorbed to high-surface ASW remain irreversibly trapped inside the ASW structure, even after the collapse of the micropore network — which is of key importance in understanding astronomical processes such as the outgassing of comets or the process of molecular evolution and planet formation. Annealing of ASW was investigated by several different experimental methods, including positron-annihilation spectroscopy [157], Brunauer-Emmett-Teller [158], electron stimulated desorption [159] and infrared reflection absorption spectroscopy [160].

Hyperquenched glassy water (HGW) is generated by depositing micrometer sized droplets with high cooling rates onto a solid substrate called “cryoplate” [161]. To that end an aerosol is introduced into a high-vacuum chamber, where nitrogen acts as a carrier gas [162]. The liquid water droplets immobilize immediately upon impact on

the cryoplate. If cooling rates of  $> 10^6$  K/s (“hyperquenching”) are reached and the cryoplate is kept at  $< 140$  K, the deposits are completely amorphous. At increasing deposition temperatures the amount of crystalline ice increases [162].

High-density amorphous ice (HDA) was produced for the first time in 1984 by Mishima *et al.* [163], using hexagonal ice as starting material. Mishima pressurized the sample to 1.6 GPa at 77 K [164] and observed a “sharp” densification step above 1.0 GPa, indicating the transformation to HDA. Since water exhibits a negatively sloped melting line it was assumed that this amorphization might resemble thermodynamic melting [164]. However, it has also been argued that this process occurs due to mechanical instability, leading to the preservation of some order in the system [165]. It has, therefore, been doubted whether HDA has a liquid-like atomistic structure [166]. The amorphous form produced along the route explained above is nowadays commonly called unannealed high-density amorphous ice (uHDA) [167]. Low-density (LDA) and very high-density amorphous ice (VHDA) can only be accessed *via* HDA. LDA is generated by heating HDA at low-pressure conditions, typically ambient pressure, to approximately 140 K [168]. Very high-density amorphous ice (VHDA) forms on isobaric heating of high-density amorphous ice (HDA) at 1.1 GPa to 165 K [169].

Amorphous ices are non-equilibrium states, which by thermodynamic necessity slowly progress towards more relaxed structures. The rate of relaxation is practically immeasurably slow, if it is kept at liquid nitrogen temperature or below. However, the time-scale for relaxation decreases to laboratory-relevant time-scales of weeks, days, hours, minutes or even seconds, if the temperature is increased to  $> 100$  K, while still avoiding crystallization, which takes place above  $\sim 150$  K at ambient pressure and above  $\sim 180$  K at 1 GPa. The effects of relaxation on amorphous ices have long been neglected entirely, and only recently became the center of interest. If uHDA is annealed at pressures between 0.3 and 0.8 GPa, it reaches states called relaxed HDA (rHDA) [170], which are of higher density than uHDA. If uHDA is annealed at  $< 0.3$  GPa [167] or if VHDA is slowly decompressed at 140 K to  $< 0.1$  GPa [171] amorphous ices of (slightly) lower-density result, which were called eHDA (expanded HDA) by Nelmes *et al.* [167]. Ambient pressure densities as determined by cryoflotation are  $0.92$  g/cm<sup>3</sup> for ASW (after micropore collapse), HGW and LDA,  $1.13$  g/cm<sup>3</sup> for eHDA,  $1.15$  g/cm<sup>3</sup> for uHDA and  $1.26$  g/cm<sup>3</sup> for VHDA.

While eHDA and uHDA are very similar in terms of atomistic structure and density, there is quite a large difference in terms of thermal stability. At ambient pressure uHDA transforms to LDA above about 110 K, whereas eHDA does not transform up to  $\sim 132$  K [151]. This difference can be rationalized in terms of the degree of intrinsic tension/relaxation. As depicted in the scheme in fig. 9, uHDA occupies high-energy states in the HDA basin of the potential energy landscape at 1 bar (blue circles), whereas eHDA represents a low-lying state, if not an equilibrated state (red circle). Because of the high-energy and less well defined nature of uHDA its transformation to the thermodynamically more stable LDA takes place at comparatively lower temperatures, and also in a broader range of temperatures than the relatively sharp transformation from eHDA to LDA at  $\sim 132$  K.

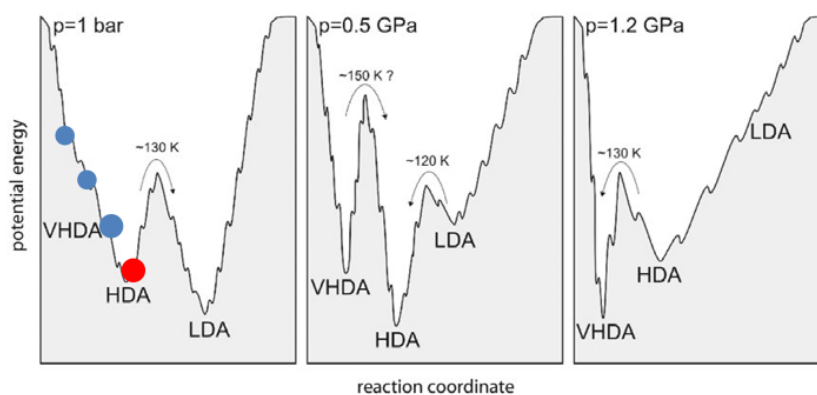


Fig. 9. – Schematic potential energy landscape of amorphous water forms at different pressures. The blue dots mark uHDA-states at 1 bar and the red dot the eHDA state. Reproduced and adapted from ref. [151].

**3.3. Atomistic structure of amorphous ices.** – The short and intermediate range order of these amorphous ices was investigated by the technique of isotope substitution neutron scattering [172]. Figure 10 depicts the pair distribution functions for the amorphous ices, where HDA refers to the uHDA state (which is quite similar to the eHDA state in terms of structure). The ASW sample was annealed *in vacuo* to 120 K to induce pore collapse [172]. A comparison of the three low-density amorphous ices (HGW, ASW and LDA) shows a striking similarity, in spite of the very different routes of preparation [172]. Just like for all crystalline ices in the pressure range up to 13 GPa, a local tetrahedral coordination is very well developed also for all amorphous ices, whereas there is barely any order at distances  $> 10 \text{ \AA}$  from the central molecule.

By contrast, HDA and VHDA differ from ASW, HGW and LDA, especially concerning the second coordination shell. The second peak in the OO-pair distribution function  $g_{OO}(r)$  shifts from about  $4.5 \text{ \AA}$  in ASW/HGW/LDA to  $4.0 \text{ \AA}$  in HDA and  $3.5 \text{ \AA}$  in VHDA. This implies that one (HDA) [173] and two (VHDA) [174] molecules from the second coordination shell move closer to the first coordination shell to so-called interstitial positions, whereas these interstitial positions are empty in case of ASW/HGW/LDA. We emphasize that these interstitial water molecules are themselves obeying the Bernal-Fowler ice rules and are tetrahedrally surrounded by four nearest neighbors [173]. At this point it is noteworthy to say that all these pair distribution functions relate to quench-recovered samples at 1 bar. Klotz *et al.* have reported *in situ* pair distribution functions, which suggest that the pair distribution function of VHDA at ambient pressure is highly similar to the pair distribution function of HDA at 100 K and 0.8 GPa [175].

**3.4. Liquid-liquid phase transition hypothesis.** – As mentioned above the pioneering studies by Mishima revealed polyamorphism in water [164, 168]. These results initiated the birth of the “liquid-liquid phase transition hypothesis” [176].

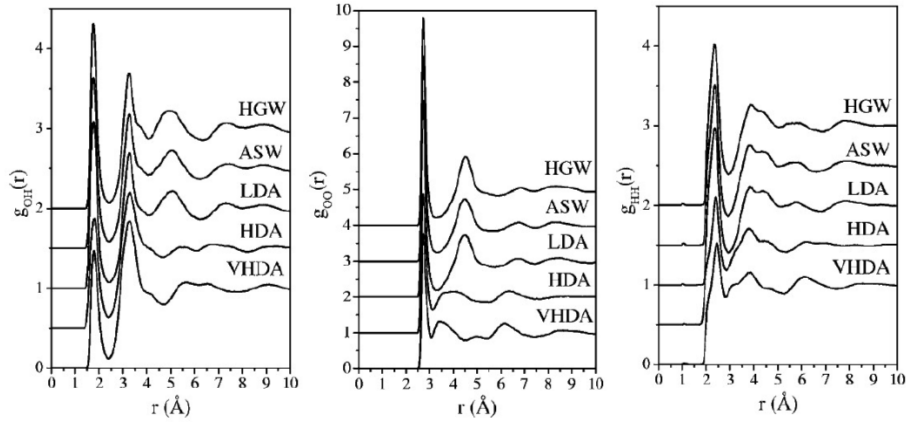


Fig. 10. – Oxygen-hydrogen, oxygen-oxygen and hydrogen-hydrogen pair distribution functions for HGW, ASW, LDA, HDA and VHDA. Reproduced from ref. [172].

Figure 11 illustrates the most stable, non-crystalline phases for water at  $< 0.35$  GPa. This diagram is dominated by a white area denoted the “No man’s land”, in which non-crystalline phases of water crystallize very rapidly, much faster than on the millisecond time-scale, so that they cannot be prepared and probed using today’s experimental techniques. The solid black line at 0.2 GPa separates LDA from HDA and represents the first-order like transition between these two phases [176]. Additionally, the low-density liquid (LDL) and high-density liquid (HDL) are depicted above the glass transition temperature  $T_g$  [176]. Understanding the one-component system water as a mixture of two distinct liquid phases would be a particularly appealing scenario for rationalizing water’s anomalies [146]. This also applies to variants of the scenario, in which there is a sharp, but continuous transition between two liquids rather than a first-order liquid-liquid transition. Studies about the glass transition of LDA and HDA and the question whether amorphous ices are proxies of supercooled liquids are necessary to make the link between amorphous ices and supercooled liquids, and they are described in the next section.

**3.5. Glass transitions in amorphous ices.** – Macroscopically a glass looks like a solid, rigid body, but microscopically its structure corresponds to a liquid — in other words a glass shows no long-range order. In general a glass is produced by undercooling a liquid below its freezing point [177]. Crystallization of a liquid during freezing can be inhibited, if the cooling rate is high enough [177]. As a result the molecules do not have enough time to arrange into the crystalline state, but retain a liquid configuration, which is frozen in [177].

The glass transition temperature can be determined by different experimental methods. One appropriate experiment is differential scanning calorimetry: it records the change of the heat capacity as a function of the temperature. At the glass transition the heat capacity changes abruptly, which is visible as an endothermic step upon heat-



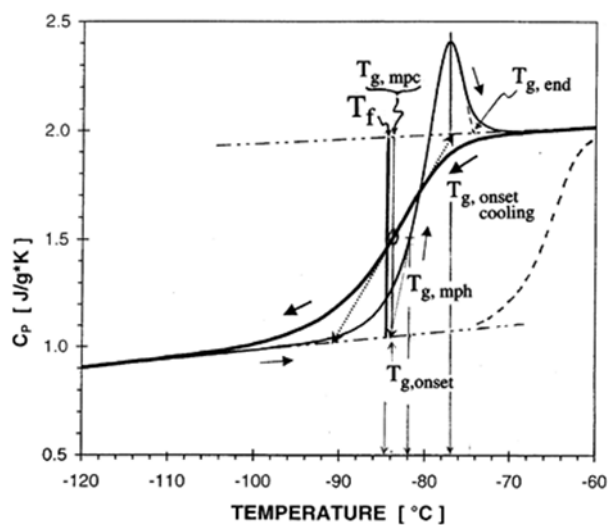


Fig. 12. – Glass transition in glycerol measured with differential scanning calorimetry (DSC) during heating and cooling. Reproduced from ref. [178].

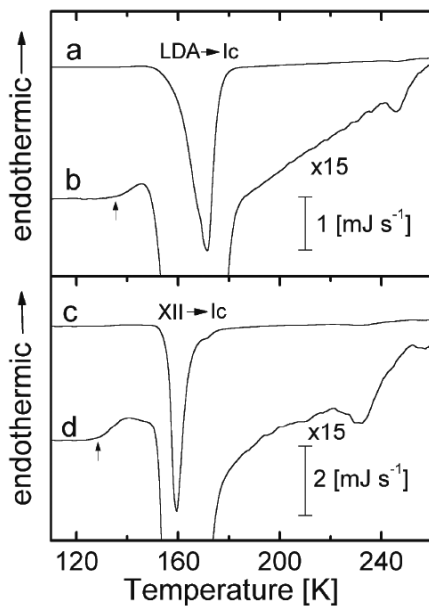


Fig. 13. – Glass transition of low-density amorphous ice (LDA) superimposed by the crystallization to cubic ice (depicted on the top). Endothermic step (transformation) in ice XII superimposed by the crystallization to cubic ice (shown on the bottom). Reproduced from ref. [74].

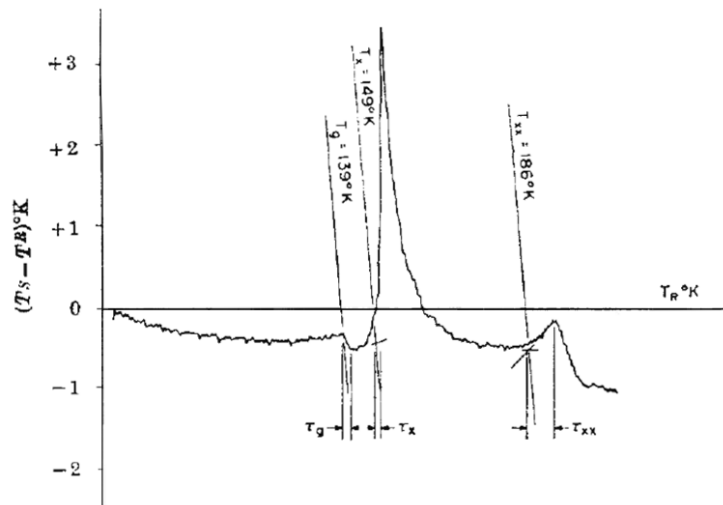


Fig. 14. – Differential thermal analysis curves for vapor deposited amorphous solid water. Reproduced from ref. [180].

This step is attributed to the onset of rotational motion in proton-disordered ice XII [74]. Annealing of the samples induces physical aging and thus relaxation to a state with lower enthalpy in the case of a glass (*e.g.*: LDA). The same holds true for annealed crystalline samples (*e.g.*: ice XII) [74]. The similarity between the calorimetric glass transition in plastic crystals (such as ice XII) and LDA prompts the question whether translational mobility indeed sets in above the calorimetric glass transition of 136 K in LDA, or in other words whether LDA transforms to LDL or another type of amorphous solid.

**3.5.1. Glass transition in ASW.** A similar question applies to ASW — this state also experiences a glass transition near 136 K, which was first detected by McMillan and Los, who utilized *in situ* differential thermal analysis to investigate vapour deposited amorphous solid water during heating [180]. For that purpose the temperature difference between the sample and a reference was recorded [180]. The warm-up curve (depicted in fig. 14) includes three important features, namely the glass transition at  $T_g$ , the crystallization to cubic ice at  $T_x$  and the crystallization to hexagonal ice  $T_{xx}$  [180]. McMillan and Los used a heating rate of 20 K/min and obtained a glass transition temperature of 139 K [180]. In contrast to the glass transition the crystallization is exothermic, where  $T_x$  is located at 149 K and  $T_{xx}$  at 186 K [180].

Later on, Sugisaki *et al.* [181] and Ghormley [182] reported on the “heat capacities of glassy water and cubic ice”. Their results show a very large increase in heat capacity, superimposed on the subtle glass transition, due to the collapse of the micropores and the massive reduction in specific surface area. This showed the need for studying well-annealed ASW, which was done in 1989 by Hallbrucker *et al.* to explore the devitrification and crystallization of ASW by DSC [183]. In order to minimize exothermic effects

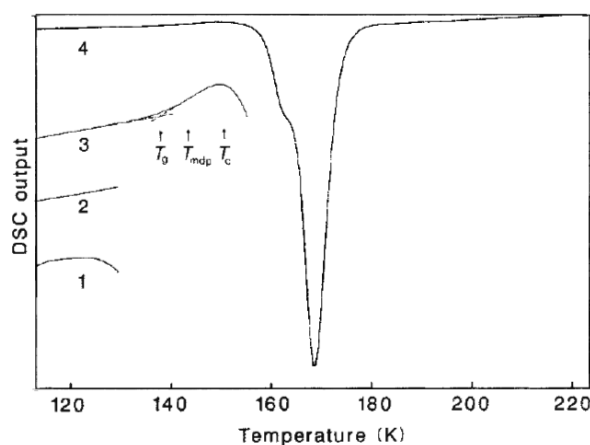


Fig. 15. – Differential scanning calorimetry curves for hyperquenched glassy water (HGW). The details for each curve are described in the text. Reproduced from ref. [184].

originating from pore sintering the ASW was annealed in the deposition apparatus to 113 K [183]. Heating this annealed sample in the DSC for the first time shows an exothermic feature due to enthalpy relaxation and further pore sintering [183]. For that reason the sample was annealed a second time in the DSC at 130 K for 90 min, and only after this the glass transition could be detected during heating [183]. Hallbrucker *et al.* showed the reversibility of the glass transition in ASW, and determined  $\Delta C_p = 1.9 \text{ JK}^{-1} \text{ mol}^{-1}$  at an onset temperature of 136 K for the glass transition (heating rate: 30 K/min) [183].

**3.5.2. Glass transition in HGW.** In 1987 Johari *et al.* reported on “the glass-liquid transition of hyperquenched water” [184]. Figure 15 illustrates the differential scanning calorimetry curves for HGW, the individual curves are described in the following step by step. A difficulty in observing a glass-to-liquid transition in HGW is the exothermic enthalpy relaxation, which is shown in curve 1. If the sample is annealed at 130 K for approximately 90 min and the DSC heating curve is recorded afterwards (curve 2) the exothermic feature arising from enthalpy relaxation is not present anymore. In order to make the “small” endothermic glass transition visible it is necessary to anneal the sample at 130 K for approximately 90 min before the heating curve is recorded. Curve 3 in fig. 15 displays the reversible glass transition in HGW on an enlarged scale. Immediately after the glass transition the crystallization to cubic ice emerges as a sharp exothermic peak. This crystallization peak superimposes the glass transition and explains the enlargement of curve 3 relative to curve 4 [184].

Yue *et al.* discuss the possibility of a shadow glass transition in HGW and ASW [185]. For that purpose the differential scanning calorimetry curves of *annealed* HGW and ASW are compared with the curves of *annealed (aged)* hyperquenched mineral glass and *unannealed (standard)* hyperquenched mineral glass. The corresponding DSC curves are illustrated in fig. 16. In the case of the standard curve the glass transition onset

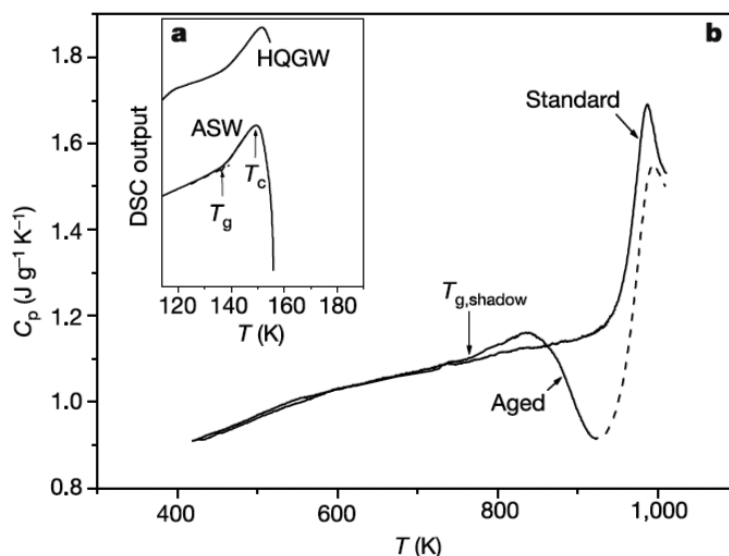


Fig. 16. – Comparison of differential scanning calorimetry curves of annealed HGW and annealed ASW (figure inset) with a scan of a hyperquenched mineral glass (standard) and with an annealed hyperquenched mineral glass (aged). Reproduced from ref. [185].

temperature is located at 944 K. Contradictory, the aged sample exhibits a much weaker endothermic feature, which occurs at 723 K. This “weak” feature is designated a shadow glass transition. The difference between an annealed and an unannealed hyperquenched glass is the release of excess enthalpy for the former one — it is able to relax. For water, the extremely small  $\Delta C_p$  (14-times smaller than the calculated value) militates in favour of a shadow glass transition according to Yue *et al.* [185]. However, Kohl *et al.* [162] studied the change of  $\Delta C_p$  as a function of different previous cooling rates at a fixed heating rate of 30 K/min, both with and without annealing at 130 K by DSC. Whereas  $\Delta C_p$  decreases with increasing cooling rate without annealing,  $\Delta C_p$  no longer depends on the previous cooling rate with an annealing step at 130 K. This argues for the equilibration of the HGW sample after 90 min at 130 K and against the continuous relaxation required if it were a shadow transition. Also, the “remarkable similarity” [79] of glass transitions between ASW, HGW and LDA argues against a shadow glass transition: LDA is not produced by a quenching route, and so it can *a priori* not experience shadow glass transitions.

**3.5.3. Glass transition in LDA.** In 1988 Handa and Klug reported for the first time on the glass transition of low-density amorphous ice (LDA) [186]. For a heating rate of 0.17 K/min Handa and Klug observed a  $\Delta C_p$  of  $0.7 \text{ JK}^{-1} \text{ mol}^{-1}$  and a glass transition temperature of 124 K [186]. Elsaesser *et al.* observed the “calorimetric glass-liquid transition of LDA” depicted in fig. 17 (curve three, arrow marked  $T_g$  at 137 K) at a heating rate of 30 K/min [79] with a  $\Delta C_p$  of  $1.7 \text{ JK}^{-1} \text{ mol}^{-1}$ . In contrast to the glass transition the crystallization is not reversible [79].

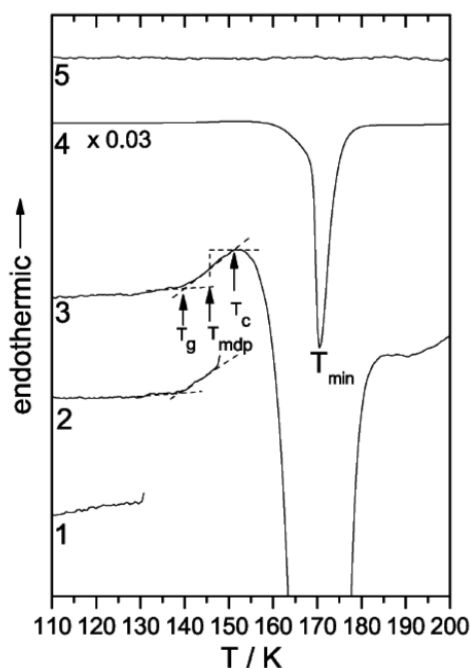


Fig. 17. – Differential scanning calorimetry curves for low-density amorphous ice (LDA) prepared from very high-density amorphous ice (VHDA). Curve 1 corresponds to heating of the sample up to 131 K and annealing it at that temperature for 90 min. Afterwards the LDA was heated to 148 K with a heating rate of 30 K/min, curve 2, and heated a third time, curves 3 and 4, from 93 K to 210 K with a heating rate of 30 K/min. Curves 3 and 4 are the same, where curve 4 is miniaturized by multiplication with 0.03. Curve 5 corresponds to the heating of cubic ice from 93 K to 210 K with a heating rate of 30 K/min. Reproduced from ref. [79].

As mentioned above the three low-density amorphous ices including ASW, HGW and LDA are structurally the same based on neutron diffraction experiments [172]. Furthermore, the differential scanning calorimetry curves exhibit a highly similar behavior, especially the onset of the glass transition located at approximately 136 K for all three ices (heating rate: 30 K/min) [79,183,184]. Some researchers have had doubts about the glass transition in low-density amorphous ices. The ideas of a “conformational” glass transition [187] and a “shadow” glass transition [185] tried to refute the concept of a “real” glass-to-liquid transition.

A study by Johari utilizing a conical indenter indicated that LDA indeed transforms into a viscous liquid near 143 K [188]. In other words, when LDA converts into the liquid it becomes deformable. By contrast the same experiment with cubic ice revealed no penetration of the indenter. Also, Smith and Kay support the idea of a glass-to-liquid transition [189]. They stated in 1999: “The amorphous solid melts into a deeply supercooled metastable extension of normal liquid water before crystallizing near 160 K”. This interpretation is based on studying isotope mixing between  $\text{H}_2^{16}\text{O}$  and  $\text{H}_2^{18}\text{O}$  deposit

layers and thereby obtaining the diffusivity of amorphous solid water. The diffusivity of stable and supercooled water follows a non-Arrhenius behavior above 235 K, which can be modeled with the Vogel-Fulcher-Tammann (VFT) equation [189]. Hence, ambient water is regarded as a “fragile” liquid. In 2006 McClure *et al.* [190] determined the diffusivity of ASW in a similar manner to Smith and Kay. In contrast to Smith and Kay the diffusivity obtained by McClure *et al.* between 150 and 160 K is much smaller. These results were explained either by a glass transition at temperatures higher than 160 K or by a fragile-to-strong transition on cooling water from 230 to 160 K. The idea of a fragile-to-strong transition in supercooled water was proposed by Ito *et al.* in 1999 [191]. They showed that the liquid, which vitrifies at 136 K, is a strong liquid. By contrast near the melting point at 273 K water is the most fragile liquid of all.

In summary, there is evidence that LDA experiences a glass transition to LDL above 136 K, and that LDL is a “strong” liquid, as opposed to water at ambient temperature. However, the discussion about this issue is certainly not settled and will continue in the future. Some experiments, which highlight similarities between LDA and crystalline, cubic ice and disfavor the transition of LDA to a liquid are summarized elsewhere [192].

**3.5.4. Glass transition in HDA.** The first studies on the possibility of a glass transition in HDA were made by Handa *et al.* They did not find any evidence for a glass transition of HDA at ambient pressure, but found that during heating HDA first relaxes, then transforms to LDA, which then further transforms to cubic ice and eventually forms hexagonal ice [77]. However, at atmospheric pressures, where Handa *et al.* conducted their experiments, HDA is not only metastable compared to the crystalline forms of ice (which might be metastable themselves as well), but also metastable compared to LDA. Thus, it would be preferable to do measurements under high pressure conditions, where HDA has a larger thermal stability and cannot transform to LDA. These types of high-pressure heat capacity measurements were technically not feasible prior to the recent *in situ* study by Andersson, who reports a reversible glass-to-liquid transition for HDA (possibly VHDA) at 1 GPa and 140 K, which is accompanied by a  $\Delta C_p$  of  $3.4 \text{ JK}^{-1} \text{ mol}^{-1}$  [193].

The question, whether HDA is a glass or not became particularly important after 1992, when Poole *et al.* published their theoretical work [194], showing that there might be a second critical point, which marks the end of a line separating the two amorphous forms LDA and HDA. Furthermore, they stated that LDA is continuously connected to the liquid, *i.e.*, a glass. This raises the question, whether HDA could also be continuously connected to the liquid and therefore exhibit a glass-to-liquid transition to a high density liquid (HDL). This question was tackled by several approaches, which can be divided into two categories, namely studies under high pressure and studies at atmospheric pressure.

First of all let us take a look at the high-pressure studies: Many experiments on HDA, including its discovery [164], were pioneered by Osamu Mishima. Mishima also conducted experiments with emulsified water, which has the advantage that one can collect data in the otherwise not accessible no-man’s land. In this region the melting line of ice IV was studied, which exhibits a melting line positively sloped with pressure, *i.e.*, it melts

upon decompression. The remarkable finding of Mishima *et al.* is that the melting line shows a kink at approximately 0.1 GPa, which is consistent with the idea of two distinct liquid forms of water [195]. Later Mishima *et al.* showed that it is possible to directly vitrify a pressurized emulsion by bringing the high-pressure equipment in contact with a cold Indium block. The resulting material was clearly amorphous and is suspected to be HDA [196]. A subsequent study on both emulsified HDA (produced by pressure-induced amorphization) and emulsified LiCl solutions showed an endothermic event upon decompression which was interpreted as a glass transition [197].

High-pressure studies using dielectric spectroscopy have been conducted by Andersson. It was shown that VHDA — Andersson regards VHDA as a form of relaxed HDA — has a dielectrical relaxation time of 1 s at 1 GPa and 140 K [198], or 100 s (the usual value at  $T_g$ ) at 122 K when heated with 15 K/h [199]. Andersson also conducted high-pressure calorimetry experiments and found a  $T_g$  of 140 K at 1 GPa when heated with 0.4 K/min [193]. A different approach was used by Seidl *et al.*, by studying the thermal expansion of both LDA at 0.006 GPa and eHDA at 0.1, 0.2 and 0.3 GPa [200]. To this end the samples were heated to a temperature below the crystallization temperature and cooled again — both with 2 K/min. This cycle was conducted several times in order to get rid of any irreversible effects that might superimpose with a possible glass transition. The curves depicted in fig. 18 show the results for LDA at 0.006 GPa and HDA at 0.2 GPa. The curves corresponding to the third and the subsequent cycles show qualitatively the same behaviour, a reversible change of slope, which was interpreted as the onset of a glass transition taking place at 144 K (0.006 GPa) for LDA and at 134 K (0.1 GPa), 140 K (0.2 GPa) and 142 K (0.3 GPa) for HDA.

All studies presented so far dealt with *in situ* approaches at high-pressures. Let us now discuss the second category of experiments, focussing on quench-recovered samples. These are samples, which have been first quenched to 77 K and then brought to atmospheric pressure, without any indications for a transformation in the course of quench-recovery. The first approach is by Handle *et al.*, who relaxed uHDA samples at 0.1 and 0.2 GPa, quenched-recovered the samples and judged the state of relaxation based on DSC measurements conducted at 1 atm [201]. uHDA samples were heated to 110, 125, 130 and 135 K with 3 K/min and kept at these temperatures isobarically and isothermally for times between 0 and  $\sim 10000$  s. After the time had elapsed the samples were quench-recovered and the transition temperature to LDA was measured with DSC at atmospheric pressure. All transition temperatures are depicted in fig. 19. One can clearly see that if annealed at 110 K the transition temperature changes only slightly, where it becomes ever higher if the annealing temperature is raised. A fit of a relaxation function to the data allows obtaining relaxation times and estimation of the  $T_g$  at the respective pressures. These estimates are 144 K for uHDA at 0.1 GPa and 150 K for uHDA at 0.2 GPa (cf. fig. 20a and b for the estimation and 20c for a summary of  $T_g$ 's found for HDA).

The next approach was to directly measure the  $T_g$  of eHDA by the means of DSC and also to conduct dielectric spectroscopy at 1 bar, which was done by Amann-Winkel *et al.* [202]. The DSC scan of eHDA shows an endothermic feature at 113 K. If the sample

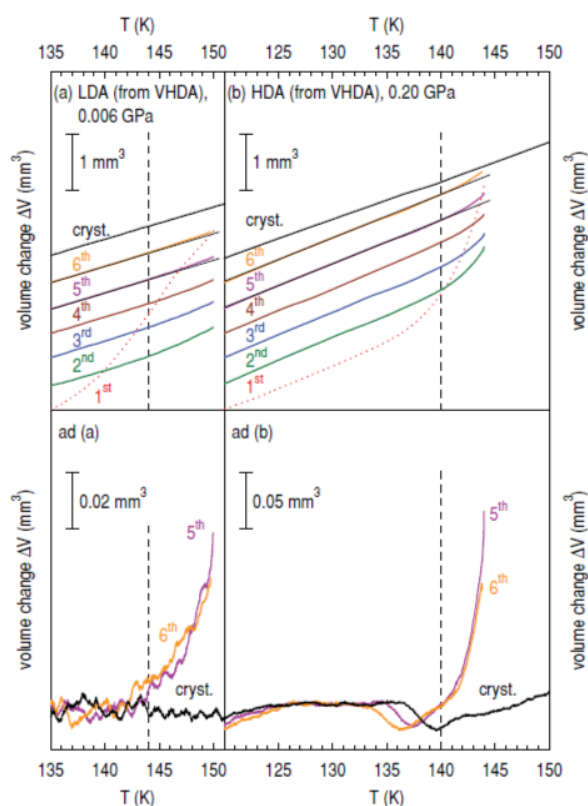


Fig. 18. – Dilatometry curves upon heating LDA at 0.006 GPa (a) and eHDA at 0.2 GPa (b). Each sample was heated and subsequently cooled with rates of 2 K/min. Dashed lines mark the deviation from linearity. The top part shows the data as measured and the bottom part was replotted after subtraction of linear fits (black lines in top part). Reproduced from ref. [200].

is cooled afterwards and heated again this endothermic event shifts to about 116 K. This effect is reversible, meaning that if the sample is cooled and heated again it exhibits the same behaviour as before (cf. fig. 21). Therefore, these events have been interpreted as the onset of the glass transition of HDA at ambient pressure. This reversible transition can be detected in eHDA, but not in uHDA. The increase in heat capacity (curve 3 in fig. 21) amounts to  $\Delta C_p = 4.8 \text{ JK}^{-1} \text{ mol}^{-1}$ . From the dielectric relaxation map a record low fragility index of  $m = 14$  was determined for LDL, putting it in the category of superstrong liquids, and a fragility of  $m = 20\text{--}25$  was determined for HDL, putting it in the category of strong liquids.

**3.6. Summary: amorphous ices.** – A range of different paths for the formation of amorphous ices in the lab, or in astrophysical environments exist. These differ in the starting material, *i.e.*, water in the vapour, liquid, or crystalline solid state, and in the

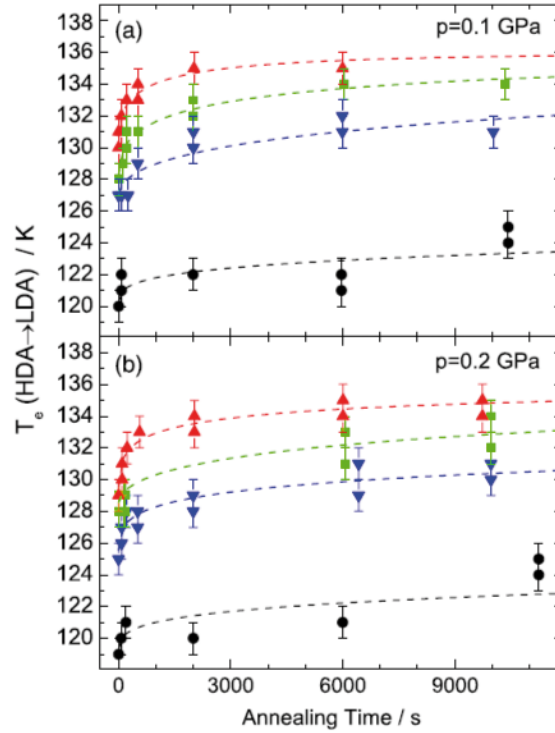


Fig. 19. – Calorimetric HDA-to-LDA transition temperatures  $T_e$  as a function of annealing time and temperature (110 K black circles, 125 K blue downward triangles, 130 K green squares, 135 K red upward triangles). The dashed lines depict the relaxation-function fits. Reproduced from ref. [201].

specific protocols employed how to cool the liquid or vapor and how to bring in the excess enthalpy into crystalline ice. In spite of amorphous ices being non-equilibrium states converging towards thermodynamic equilibrium, there are exactly three distinct categories of amorphous ices, in which they can be viewed as metastable “phases”. Low- (LDA), high- (HDA) and very high-density amorphous ice (VHDA) are the most stable non-crystalline forms of ice at  $< 0.1$  GPa, 0.1–0.8 GPa and  $> 0.8$  GPa, respectively. Recent studies have shown that amorphous ices can in fact be equilibrated, without conversion to the crystalline state, provided the temperature is kept sufficiently below  $T_x$ . Equilibration times, structural relaxation times and dielectric relaxation times can be reduced to less than 100 seconds by heating them to  $T < T_x$ , both for LDA at ambient pressure and HDA at intermediate-pressure conditions. This suggests that the amorphous ices transform to deeply supercooled, ultraviscous liquid prior to crystallization. In case of HDA the relaxed eHDA state (as opposed to the uHDA state originally discovered by Mishima) even allows to observe the glass-to-liquid transition at ambient pressure, prior to the transformation to LDA. The observation of two distinct glass transitions of amor-

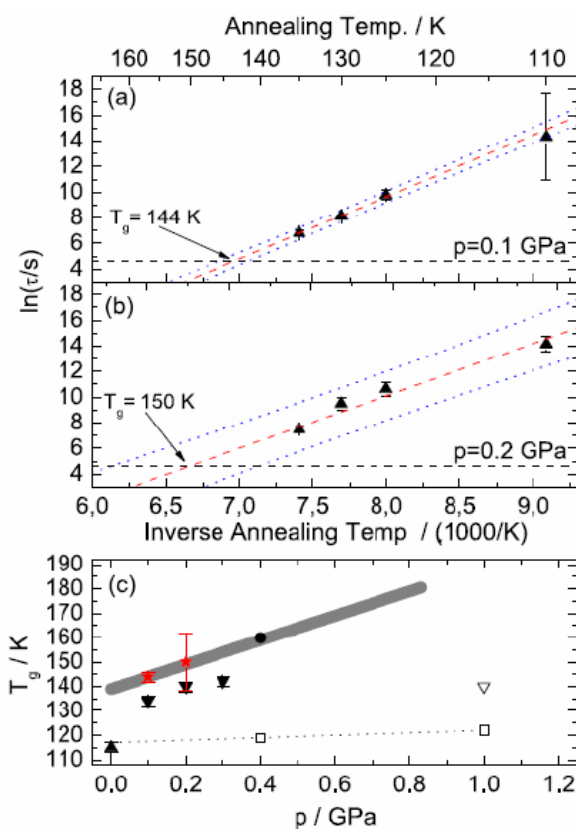


Fig. 20. – Arrhenius plots with a corresponding fit (red dashed line) of the relaxation times calculated from the data depicted in fig. 19 for 0.1 GPa (a) and 0.2 GPa (b). The black dashed line marks a relaxation time of 100 s and the extrapolated  $T_g$ 's are marked by arrows. Part (c) shows a summary of glass transition temperatures for HDA obtained by Handle *et al.* [201] as explained above (red stars), Amann-Winkel *et al.* [202], calorimetry (black upward triangle); Seidl *et al.* [200], volumetry (black downward triangles); Andersson, transient hot-wire method [193] (open downward triangle); Mishima, endothermic event in emulsified water [197] (black circle) and grey area (data from LiCl emulsions); Andersson and Inaba, dielectric spectroscopy [199] (open squares) and dotted line (Andersson's extrapolation). Reproduced from ref. [201].

phous ices at ambient pressure, separated by about 20 K, favours a double-liquid and a double- $T_g$  scenario for our understanding of water. However, the debate will certainly continue whether there are one, two or maybe even three liquids of water. The possibility of VHDA being connected to VHDL was not studied at all so far, but will need to be in the future. One way of answering these questions will be the study of aqueous solutions at extreme conditions, especially in the dilute regime and extrapolating to the pure water case. For instance, calorimetric and X-ray diffraction studies done in LiCl–H<sub>2</sub>O systems

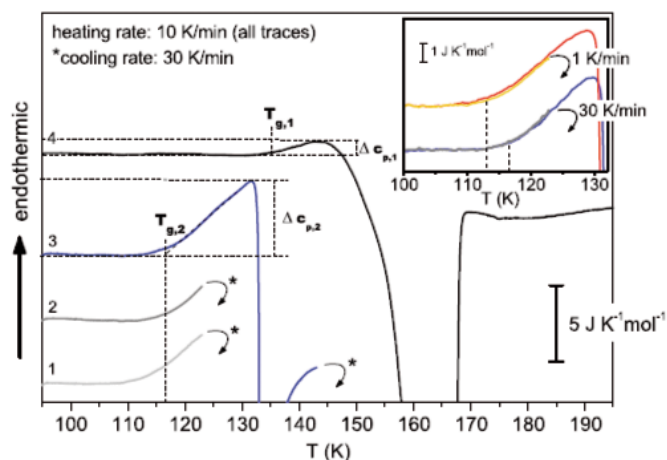


Fig. 21. – DSC measurements of eHDA. The sample was heated with 10 K/min to 123 K (1) then cooled at 30 K/min to 90 K. This procedure was repeated (2) and then the sample was heated with the same rate to 145 K (3) and cooled again (same rates). Thereafter the sample was heated to 253 K (4).  $T_{g,1}$  and  $T_{g,2}$  mark the glass transition temperature for LDA and HDA respectively. The inset shows the change in  $T_{g,2}$  as a function of cooling rate – 1 K/min vs. 30 K/min. Reproduced from ref. [202].

on uHDA and eHDA samples produced by pressure-induced amorphization show clues on the existence of LDL and HDL and their connection to LDA and HDA [203]. The DSC study of LDA samples, produced by isobaric heating of eHDA of concentrations between 0.00 and 0.12 LiCl mole fraction, shows a plateau region around 150–155 K after the LDA glass transition and before crystallization, which is not evident in pure water. The absence of this plateau region in the DSC scans shown in this review article has always fuelled the debate about whether or not a liquid state is reached upon heating amorphous ices. The appearance of this region in dilute salt solution allows for the affirmation of the appearance of a low-density liquid. Similarly, a second plateau region could be observed in DSC scans of pressure-amorphized dilute LiCl solutions after the HDA glass transition and prior to transformation into a low-density phase, which affirms the notion of the appearance of the high-density liquid, even at ambient pressure [203].

\* \* \*

Our work on water is supported by the Austrian Science Fund FWF (START award Y391 and French-Austrian bilateral project I1392), the European Research Council ERC (Starting Grant SULIWA), the Alexander von Humboldt foundation (Friedrich Wilhelm Bessel Research Award to T.L.) and the Austrian Academy of Sciences ÖAW (DOC fellowship to M.S.).

## REFERENCES

- [1] HOBBS P. V., *Ice Physics* (Clarendon Press, Oxford) 1974.
- [2] BERNSTEIN J., *Polymorphism in Molecular Crystals* (Oxford University Press, Oxford, UK) 2002.
- [3] KLAPROTH M. H., *Bergmannische J.*, **I** (1798) 294.
- [4] MITSCHERLICH E., *Abhl. Akad. Berlin*, (1822-1823) 43.
- [5] ZHELIGOVSKAYA E. A., and MALENKOV G. G., *Russ. Chem. Rev.*, **75** (2006) 57.
- [6] MALENKOV G., *J. Phys.: Condens. Matter*, **21** (2009) 283101.
- [7] FORTES A. D., WOOD I. G., VOCADLO L., KNIGHT K. S., MARSHALL W. G., TUCKER M. G., and FERNANDEZ-ALONSO F., *J. Appl. Crystallogr.*, **42** (2009) 846.
- [8] FORTES A. D. and CHOUKROUN M., *Space Sci. Rev.*, **153** (2010) 185.
- [9] MCFARLAN R. L., *J. Chem. Phys.*, **4** (1936) 253.
- [10] KAMB B. and PRAKASH A., *Acta Crystallogr., Sect. B*, **24** (1968) 1317.
- [11] KAMB B., PRAKASH A. and KNOBLER C., *Acta Crystallogr.*, **22** (1967) 706.
- [12] KAMB B., *Science*, **150** (1965) 205.
- [13] KAMB B. and DAVIS B. L., *Proc. Natl. Acad. Sci. U.S.A.*, **52** (1964) 1433.
- [14] BERTIE J. E., CALVERT L. D. and WHALLEY E., *Can. J. Chem.*, **42** (1964) 1373.
- [15] KLOTZ S., BESSON J. M., HAMEL G., NELMES R. J., LOVEDAY J. S. and MARSHALL W. G., *Nature*, **398** (1999) 681.
- [16] SCHWAGER B., CHUDINOVSKIKH L., GAVRILIUK A. and BOEHLER R., *J. Phys.: Condens. Matter*, **16** (2004) S1177.
- [17] GONCHAROV A. F., GOLDMAN N., FRIED L. E., CROWHURST J. C., KUO I. F. W., MUNDY C. J. and ZAUG J. M., *Phys. Rev. Lett.*, **94** (2005) 125508.
- [18] KAMB B., *Acta Crystallogr.*, **17** (1964) 1437.
- [19] KAMB B., HAMILTON W. C., LAPLACA S. J. and PRAKASH A., *J. Chem. Phys.*, **55** (1971) 1934.
- [20] FINCH E. D., RABIDEAU S. W., WENZEL R. G. and NERESON N. G., *J. Chem. Phys.*, **49** (1968) 4361.
- [21] FORTES A. D., WOOD I. G., BRODHOLT J. P. and VOCADLO L., *J. Chem. Phys.*, **119** (2003) 4567.
- [22] FORTES A. D., WOOD I. G., ALFREDSSON M., VOCADLO L. and KNIGHT K. S., *J. Appl. Crystallogr.*, **38** (2005) 612.
- [23] WHALLEY E., DAVIDSON D. W. and HEATH J. B. R., *Chem. Phys.*, **45** (1966) 3976.
- [24] KUHS W. F., FINNEY J. L., VETTIER C. and BLISS D. V., *J. Chem. Phys.*, **81** (1984) 3612.
- [25] JORGENSEN J. D., BEYERLEIN R. A., WATANABE N. and WORLTON T. G., *J. Chem. Phys.*, **81** (1984) 3211.
- [26] JORGENSEN J. D. and WORLTON T. G., *J. Chem. Phys.*, **83** (1985) 329.
- [27] PRUZAN P., CHERVIN J. C. and GAUTHIER M., *Europhys. Lett.*, **13** (1990) 81.
- [28] PRUZAN P., CHERVIN J. C. and CANNY B., *J. Chem. Phys.*, **97** (1992) 718.
- [29] BESSON J. M., PRUZAN P., KLOTZ S., HAMEL G., SILVI B., NELMES R. J., LOVEDAY J. S., WILSON R. M. and HULL S., *Phys. Rev. B*, **49** (1994) 12540.
- [30] BESSON J. M., KOBAYASHI M., NAKAI T., ENDO S. and PRUZAN P., *Phys. Rev. B*, **55** (1997) 11191.
- [31] PRUZAN P., CHERVIN J. C., WOLANIN E., CANNY B., GAUTHIER M. and HANFLAND M., *J. Raman Spectrosc.*, **34** (2003) 591.
- [32] SONG M., YAMAWAKI H., FUJIHISA H., SAKASHITA M. and AOKI K., *Phys. Rev. B*, **68** (2003) 014106.
- [33] SINGER S. J., KUO J.-L., HIRSCH T. K., KNIGHT C., OJAMAE L. and KLEIN M. L., *Phys. Rev. Lett.*, **94** (2005) 135701.

- [34] KNIGHT C., SINGER S. J., KUO J.-L., HIRSCH T. K., OJAMAE L. and KLEIN M. L., *Phys. Rev. E*, **73** (2006) 056113.
- [35] YOSHIMURA Y., STEWART S. T., SOMAYAZULU M., MAO H.-K. and HEMLEY R. J., *J. Chem. Phys.*, **124** (2006) 024502.
- [36] SOMAYAZULU M., SHU J., ZHA C.-S., GONCHAROV A. F., TSCHAUNER O., MAO H.-K. and HEMLEY R. J., *J. Chem. Phys.*, **128** (2008) 064510.
- [37] FAN X., BING D., ZHANG J., SHEN Z. and KUO J.-L., *Comp. Mater. Sci.*, **49** (2010) S170.
- [38] TAJIMA Y., MATSUO T. and SUGA H., *J. Phys. Chem. Solids*, **45** (1984) 1135.
- [39] MATSUO T., TAJIMA Y. and SUGA H., *J. Phys. Chem. Solids*, **47** (1986) 165.
- [40] FUKAZAWA H., IKEDA S. and MAE S., *Chem. Phys. Lett.*, **282** (1998) 215.
- [41] FUKAZAWA H., IKEDA S., OGURO M., FUKUMURA T. and MAE S., *J. Phys. Chem. B*, **106** (2002) 6021.
- [42] KUO J.-L., KLEIN M. L. and KUHS W. F., *J. Chem. Phys.*, **123** (2005) 134505.
- [43] KUHS W. F., LOBBAN C. and FINNEY J. L., *Rev. High Pressure Sci. Technol.*, **7** (1998) 1141.
- [44] LOBBAN C., FINNEY J. L. and KUHS W. F., *J. Chem. Phys.*, **112** (2000) 7169.
- [45] SALZMANN C. G., RADAELLI P. G., HALLBRUCKER A., MAYER E. and FINNEY J. L., *Science*, **311** (2006) 1758.
- [46] SALZMANN C. G., HALLBRUCKER A., FINNEY J. L. and MAYER E., *Phys. Chem. Chem. Phys.*, **8** (2006) 3088.
- [47] SALZMANN C. G., RADAELLI P. G., FINNEY J. L. and MAYER E., *Phys. Chem. Chem. Phys.*, **10** (2008) 6313.
- [48] KNIGHT C. and SINGER S. J., *J. Chem. Phys.*, **129** (2008) 164513.
- [49] SALZMANN C. G., HALLBRUCKER A., FINNEY J. L. and MAYER E., *Chem. Phys. Lett.*, **429** (2006) 469.
- [50] TRIBELLO G. A., SLATER B. and SALZMANN C. G., *J. Am. Chem. Soc.*, **128** (2006) 12594.
- [51] KNIGHT C. and SINGER S. J., *J. Phys. Chem. B*, **109** (2005) 21040.
- [52] KUO J.-L. and KUHS W. F., *J. Phys. Chem. B*, **110** (2006) 3697.
- [53] SALZMANN C. G., RADAELLI P. G., MAYER E. and FINNEY J. L., *Phys. Rev. Lett.*, **103** (2009) 105701.
- [54] BAUER M., ELSAESSER M. S., WINKEL K., MAYER E. and LOERTING T., *Phys. Rev. B*, **77** (2008) 220105.
- [55] WHALLEY E., HEATH J. B. R. and DAVIDSON D. W., *J. Chem. Phys.*, **48** (1968) 2362.
- [56] LAPLACA S. J., HAMILTON W. C., KAMB B. and PRAKASH A., *J. Chem. Phys.*, **58** (1973) 567.
- [57] NISHIBATA K. and WHALLEY E., *J. Chem. Phys.*, **60** (1974) 3189.
- [58] MINCEVA-SUKAROVA B., SHERMAN W. F. and WILKINSON G. R., *J. Mol. Struct.*, **115** (1984) 137.
- [59] LONDONO J. D., KUHS W. F. and FINNEY J. L., *J. Chem. Phys.*, **98** (1993) 4878.
- [60] KNIGHT C. and SINGER S. J., *J. Chem. Phys.*, **125** (2006) 064506.
- [61] ENGELHARDT H. and WHALLEY E., *J. Chem. Phys.*, **56** (1972) 2678.
- [62] ENGELHARDT H. and KAMB B., *J. Chem. Phys.*, **75** (1981) 5887.
- [63] SALZMANN C. G., LOERTING T., KOHL I., MAYER E. and HALLBRUCKER A., *J. Phys. Chem. B*, **106** (2002) 5587.
- [64] SALZMANN C. G., KOHL I., LOERTING T., MAYER E. and HALLBRUCKER A., *Can. J. Phys.*, **81** (2003) 25.
- [65] SALZMANN C. G., MAYER E. and HALLBRUCKER A., *Phys. Chem. Chem. Phys.*, **6** (2004) 1269.
- [66] LOBBAN C., FINNEY J. L. and KUHS W. F., *Nature*, **391** (1998) 268.

- [67] O'KEEFFE M., *Nature*, **392** (1998) 879.
- [68] HALLBRUCKER A., in *Metastable Water*, edited by GEIGER A. and H.-D. (Lüdemann International Bunsen Discussion Meeting, Schloss Nordkirchen, Germany, 1999).
- [69] KOZA M., SCHOBER H., TÖLLE A., FUJARA F. and HANSEN T., *Nature*, **397** (1999) 660.
- [70] KOZA M. M., SCHOBER H., HANSEN T., TÖLLE A. and FUJARA F., *Phys. Rev. Lett.*, **84** (2000) 4112.
- [71] KOHL I., MAYER E. and HALLBRUCKER A., *J. Phys. Chem. B*, **104** (2000) 12102.
- [72] KOHL I., MAYER E. and HALLBRUCKER A., *Phys. Chem. Chem. Phys.*, **3** (2001) 602.
- [73] LOERTING T., KOHL I., SALZMANN C., MAYER E. and HALLBRUCKER A., *J. Chem. Phys.*, **116** (2002) 3171.
- [74] SALZMANN C. G., KOHL I., LOERTING T., MAYER E. and HALLBRUCKER A., *Phys. Chem. Chem. Phys.*, **5** (2003) 3507.
- [75] DOWELL L. G. and RINFRET A. P., *Nature*, **188** (1960) 1144.
- [76] MURRAY B. J., KNOPF D. A. and BERTRAM A. K., *Nature*, **434** (2005) 202.
- [77] HANDA Y. P., MISHIMA O. and WHALLEY E., *J. Chem. Phys.*, **84** (1986) 2766.
- [78] HANDA Y. P., KLUG D. D. and WHALLEY E., *J. Phys. (Paris) Colloq.*, **48** (1987) 435.
- [79] ELSAESSER M. S., WINKEL K., MAYER E. and LOERTING T., *Phys. Chem. Chem. Phys.*, **12** (2010) 708.
- [80] RAMIREZ R., NEUERBURG N. and HERRERO C. P., *J. Chem. Phys.*, **139** (2013) 084503.
- [81] SANZ E., VEGA C., ABASCAL J. L. F. and MACDOWELL L. G., *Phys. Rev. Lett.*, **92** (2004) 255701.
- [82] EVANS L. F., *J. Appl. Phys.*, **38** (1967) 4930.
- [83] KOHL I., LOERTING T., SALZMANN C., MAYER E. and HALLBRUCKER A., *NATO Sci. Ser., II: Math. Phys. Chem.*, **81** (2002) 325.
- [84] SALZMANN C., KOHL I., LOERTING T., MAYER E. and HALLBRUCKER A., *J. Phys. Chem. B*, **106** (2002) 1.
- [85] PETRENKO V. F. and WHITWORTH R. W., *Physics of Ice* (Oxford University Press, Oxford) 1999.
- [86] WHALLEY E., *J. Phys. Chem.*, **87** (1983) 4174.
- [87] MAYER E. and HALLBRUCKER A., *Nature (London)*, **325** (1987) 601.
- [88] HANDA Y. P., KLUG D. D. and WHALLEY E., *J. Chem. Phys.*, **84** (1986) 7009.
- [89] HALLBRUCKER A. and MAYER E., *J. Phys. Chem.*, **91** (1987) 503.
- [90] TANAKA H. and OKABE I., *Chem. Phys. Lett.*, **259** (1996) 593.
- [91] KUHS W. F., BLISS D. V. and FINNEY J. L., *J. Phys. (Paris) Colloq.*, **48** (1987) C631.
- [92] GUINIER A., BOKII G. B., BOLL-DORNBERGER K., COWLEY J. M., DUROVIC S., JAGODZINSKI H., KRISHNA P., DE WOLFF P. M., ZVYAGIN B. B. *et al.*, *Acta Crystallogr.*, **A40** (1984) 399.
- [93] KUHS W. F. and LEHMANN M. S., in *Water Science Reviews 2*, edited by FRANKS F. (Cambridge University Press, Cambridge) 1986, p. 1.
- [94] RÖTTGER K., ENDRISS A., IHRINGER J., DOYLE S. and KUHS W. F., *Acta Crystallogr.*, **B50** (1994) 644.
- [95] KOHL I., MAYER E. and HALLBRUCKER A., *Phys. Chem. Chem. Phys.*, **2** (2000) 1579.
- [96] HANSEN T. C., FALENTY A. and KUHS W. F., in *Physics and Chemistry of Ice*, edited by KUHS W. F., Vol. **311** (Royal Society of Chemistry) 2007, pp. 201–20.
- [97] PATTERSON M. S., *J. Appl. Phys.*, **23** (1952) 805.
- [98] HANSEN T. C., KOZA M. M., LINDNER P. and KUHS W. F., *J. Phys.: Condens. Matter*, **20** (2008) 285105.
- [99] HANSEN T. C., KOZA M. M. and KUHS W. F., *J. Phys.: Condens. Matter*, **20** (2008) 285104.
- [100] MARTIN-CONDE M., MACDOWELL L. G. and VEGA C., *J. Chem. Phys.*, **125** (2006) 116101.

- [101] NOYA E. G., CONDE M. M. and VEGA C., *J. Chem. Phys.*, **129** (2008) 104704.
- [102] BERNAL J. D. and FOWLER R. H., *J. Chem. Phys.*, **1** (1933) 515.
- [103] LOKOTOSH T. V. and MALOMUZH N. P., *Khim. Fiz.*, **12** (1993) 897.
- [104] ZABRODSKY V. G. and LOKOTOSH T. V., *Ukr. Fiz. Zh.*, **38** (1993) 1714.
- [105] PAULING L., *J. Am. Chem. Soc.*, **57** (1935) 2680.
- [106] HOLZAPFEL W. B., *J. Chem. Phys.*, **56** (1972) 712.
- [107] POLIAN A. and GRIMSDITCH M., *Phys. Rev. Lett.*, **52** (1984) 1312.
- [108] POLIAN A., BESSON J. M. and GRIMSDITCH M., *Solid state physics under pressure: recent advances with anvil devices*, edited by MINOMURA S. (High Pressure Institute of Japan, 1985) p. 93.
- [109] TEIXEIRA J., *Nature*, **392** (1998) 232.
- [110] HIRSCH K. R. and HOLZAPFEL W. B., *Phys. Lett. A*, **101** (1984) 142.
- [111] HIRSCH K. R. and HOLZAPFEL W. B., *J. Chem. Phys.*, **84** (1986) 2771.
- [112] AOKI K., YAMAWAKI H., SAKASHITA M. and FUJIHISA H., *Phys. Rev. B*, **54** (1996) 15673.
- [113] SONG M., YAMAWAKI H., FUJIHISA H., SAKASHITA M. and AOKI K., *Phys. Rev. B*, **60** (1999) 12644.
- [114] KATOH E., SONG M., YAMAWAKI H., FUJIHISA H., SAKASHITA M. and AOKI K., *Phys. Rev. B*, **62** (2000) 2976.
- [115] BENOIT M., MARX D. and PARRINELLO M., *Nature*, **392** (1998) 258.
- [116] PRUZAN P., WOLANIN E., GAUTHIER M., CHERVIN J. C., CANNY B., HAEUSERMANN D. and HANFLAND M., *J. Phys. Chem. B*, **101** (1997) 6230.
- [117] HEMLEY R. J., JEPHCOAT A. P., MAO H. K., ZHA C. S., FINGER L. W. and COX D. E., *Nature*, **330** (1987) 737.
- [118] BENOIT M., MARX D. and PARRINELLO M., *Solid State Ionics*, **125** (1999) 23.
- [119] GONCHAROV A. F., STRUZHUKIN V. V., SOMAYAZULU M. S., HEMLEY R. J. and MAO H. K., *Science*, **273** (1996) 218.
- [120] GONCHAROV A. F., STRUZHUKIN V. V., MAO H.-K. and HEMLEY R. J., *Phys. Rev. Lett.*, **83** (1999) 1998.
- [121] GUTHRIE M., BOEHLER R., TULK C. A., MOLAISON J. J., DOS SANTOS A. M., LI K. and HEMLEY R. J., *Proc. Natl. Acad. Sci. U.S.A.*, **110** (2013) 10552.
- [122] BENOIT M., BERNASCONI M., FOCHER P. and PARRINELLO M., *Phys. Rev. Lett.*, **76** (1996) 2934.
- [123] MARQUES M., ACKLAND G. J. and LOVEDAY J. S., *High Pressure Res.*, **29** (2009) 208.
- [124] CARACAS R., *Phys. Rev. Lett.*, **101** (2008) 085502.
- [125] DEMONTIS P., LESAR R. and KLEIN M. L., *Phys. Rev. Lett.*, **60** (1988) 2284.
- [126] DEMONTIS P., KLEIN M. L. and LESAR R., *Phys. Rev. B*, **40** (1989) 2716.
- [127] MILITZER B. and WILSON H. F., *Phys. Rev. Lett.*, **105** (2010) 195701.
- [128] CAVAZZONI C., CHIAROTTI G. L., SCANDOLO S., TOSATTI E., BERNASCONI M. and PARRINELLO M., *Science*, **283** (1999) 44.
- [129] IMRE A. R., DROZD-RZOSKA A., HORVATH A., KRASKA T. and RZOSKA S. J., *J. Non-Cryst. Solids*, **354** (2008) 4157.
- [130] HENDERSON S. J. and SPEEDY R. J., *J. Phys. Chem.*, **91** (1987) 3069.
- [131] HERBERT E., BALIBAR S. and CAUPIN F., *Phys. Rev. E*, **74** (2006) 041603.
- [132] ZHENG Q., DURBEN D. J., WOLF G. H. and ANGELL C. A., *Science*, **254** (1991) 829.
- [133] ZHENG Q., GREEN J., KIEFFER J., POOLE P. H., SHAO J., WOLF G. H. and ANGELL C. A., *NATO Sci. Ser., II: Math. Phys. Chem.*, **84** (2002) 33.
- [134] ROEDDER E., *Science*, **155** (1967) 1413.
- [135] CONDE M. M., VEGA C., TRIBELLO G. A. and SLATER B., *J. Chem. Phys.*, **131** (2009) 034510.

- [136] DAVIDSON D. W., in *Water - A Comprehensive Treatise*, edited by FRANKS F. (Plenum Press) 1973, p. 15.
- [137] STROBEL T. A., HESTER K. C., KOH C. A., SUM A. K. and SLOAN E. D. jr., *Chem. Phys. Lett.*, **478** (2009) 97.
- [138] JACOBSON L. C., HUJO W. and MOLINERO V., *J. Phys. Chem. B*, **113** (2009) 10298.
- [139] KOSYAKOV V. I., *J. Struct. Chem.*, **50** (2009) S60.
- [140] FENNEL C. J. and GEZELTER J. D., *J. Chem. Theory Comput.*, **1** (2005) 662.
- [141] VEGA C., SANZ E., ABASCAL J. L. F. and NOYA E. G., *J. Phys.: Condens. Matter*, **20** (2008) 153101.
- [142] MCMILLAN P. F., *Chem. Commun.*, (2003) 919.
- [143] FRASER H. J., COLLINGS M. P., MCCOUSTRA M. R. S. and WILLIAMS D. A., *Mon. Not. R. Astron. Soc.*, **327** (2001) 1165.
- [144] MURRAY B. J. and JENSEN E. J., *J. Atmos. Solar-Terrest. Phys.*, **72** (2010) 51.
- [145] BINA C. R. and NAVROTSKY A., *Nature*, **408** (2000) 844.
- [146] DEBENEDETTI P. G., *J. Phys.: Condens. Matter*, **15** (2003) R1669.
- [147] MISHIMA O., *Proc. Jpn. Acad., Ser. B*, **86** (2010) 165.
- [148] ANGELL C. A., *Annu. Rev. Phys. Chem.*, **55** (2004) 559.
- [149] LOERTING T. and GIOVAMBATTISTA N., *J. Phys.: Condens. Matter*, **18** (2006) R919.
- [150] LOERTING T., BRAZHUKIN V. V. and MORISHITA T., *Adv. Chem. Phys.*, **143** (2009) 29.
- [151] LOERTING T., WINKEL K., SEIDL M., BAUER M., MITTERDORFER C., HANDLE P. H., SALZMANN C. G., MAYER E., FINNEY J. L. and BOWRON D. T., *Phys. Chem. Chem. Phys.*, **13** (2011) 8783.
- [152] BURTON E. F. and OLIVER W. F., *Nature*, **135** (1935) 505.
- [153] MAYER E. and PLETZER R., *Nature*, **319** (1986) 298.
- [154] EHRENFREUND P., FRASER H. J., BLUM J., CARTWRIGHT J. H. E., GARCIA-RUIZ J. M., HADAMCIK E., LEVASSEUR-REGOURD A. C., PRICE S., PRODI F. and SARKISSIAN A., *Planetary Space Sci.*, **51** (2003) 473.
- [155] STEVENSON K. P., KIMMEL G. A., DOHNALEK Z., SMITH R. S. and KAY B. D., *Science*, **283** (1999) 1505.
- [156] BARAGIOLA R. A., in *Water in Confining Geometries*, edited by BUCH V. and DEVLIN J. P. (Springer-Verlag, Heidelberg) 2003, p. 359.
- [157] WU Y. C., KALLIS A., JIANG J. and COLEMAN P. G., *Phys. Rev. Lett.*, **105** (2010) 066103.
- [158] BOXE C. S., BODSGARD B. R., SMYTHE W. and LEU M. T., *J. Colloid Interface Sci.*, **309** (2007) 412.
- [159] TRONC M. and AZRIA R., *Int. J. Mass Spectrom.*, **205** (2001) 325.
- [160] HORIMOTO N., KATO H. S. and KAWAI M., *J. Chem. Phys.*, **116** (2002) 4375.
- [161] MAYER E., *J. Appl. Phys.*, **58** (1985) 663.
- [162] KOHL I., BACHMANN L., HALLBRUCKER A., MAYER E. and LOERTING T., *Phys. Chem. Chem. Phys.*, **7** (2005) 3210.
- [163] MISHIMA O., CALVERT L. D. and WHALLEY E., *J. Phys. Colloq.*, **C8** (1984) 239.
- [164] MISHIMA O., CALVERT L. D. and WHALLEY E., *Nature*, **310** (1984) 393.
- [165] TSE J. S., *J. Chem. Phys.*, **96** (1992) 5482.
- [166] TSE J. S., KLUG D. D., TULK C. A., SWAINSON I., SVENSSON E. C., LOONG C. K., SHPAKOV V., BELOSLUDOV V. R., BELOSLUDOV R. V. and KAWAZOE Y., *Nature*, **400** (1999) 647.
- [167] NELMES R. J., LOVEDAY J. S., STRAESSLE T., BULL C. L., GUTHRIE M., HAMEL G. and KLOTZ S., *Nat. Phys.*, **2** (2006) 414.
- [168] MISHIMA O., CALVERT L. D. and WHALLEY E., *Nature*, **314** (1985) 76.
- [169] LOERTING T., SALZMANN C., KOHL I., MAYER E. and HALLBRUCKER A., *Phys. Chem. Chem. Phys.*, **3** (2001) 5355.

- [170] SALZMANN C. G., LOERTING T., KLOTZ S., MIRWALD P. W., HALLBRUCKER A. and MAYER E., *Phys. Chem. Chem. Phys.*, **8** (2006) 386.
- [171] WINKEL K., ELSAESSER M. S., MAYER E. and LOERTING T., *J. Chem. Phys.*, **128** (2008) 044510.
- [172] BOWRON D. T., FINNEY J. L., HALLBRUCKER A., KOHL I., LOERTING T., MAYER E. and SOPER A. K., *J. Chem. Phys.*, **125** (2006) 194502.
- [173] FINNEY J. L., HALLBRUCKER A., KOHL I., SOPER A. K. and BOWRON D. T., *Phys. Rev. Lett.*, **88** (2002) 225503.
- [174] FINNEY J. L., BOWRON D. T., SOPER A. K., LOERTING T., MAYER E. and HALLBRUCKER A., *Phys. Rev. Lett.*, **89** (2002) 205503.
- [175] KLOTZ S., STRAESSLE T., SAITTA A. M., ROUSSE G., HAMEL G., NELMES R. J., LOVEDAY J. S. and GUTHRIE M., *J. Phys.: Condens. Matter*, **17** (2005) S967.
- [176] STANLEY H. E., BULDYREV S. V., CANPOLAT M., MISHIMA O., SADR-LAHIJANY M. R., SCALA A. and STARR F. W., *Phys. Chem. Chem. Phys.*, **2** (2000) 1551.
- [177] JOHARI G. P., *J. Chem. Edu.*, **51** (1974) 23.
- [178] ANGELL C. A., *Chem. Rev.*, **102** (2002) 2627.
- [179] SUGA H., *Thermochim. Acta*, **245** (1994) 69.
- [180] McMILLAN J. A. and LOS S. C., *Nature*, **206** (1965) 806.
- [181] SUGISAKI M., SUGA H. and SEKI S., *Bull. Chem. Soc. J.*, **41** (1968) 2591.
- [182] GHORMLEY J. A., *J. Chem. Phys.*, **48** (1968) 503.
- [183] HALLBRUCKER A., MAYER E. and JOHARI G. P., *J. Phys. Chem.*, **93** (1989) 4986.
- [184] JOHARI G. P., HALLBRUCKER A. and MAYER E., *Nature*, **330** (1987) 552.
- [185] YUE Y. and ANGELL C. A., *Nature*, **427** (2004) 717.
- [186] HANDA Y. P. and KLUG D. D., *J. Phys. Chem.*, **92** (1988) 3323.
- [187] FISHER M. and DEVLIN J. P., *J. Phys. Chem.*, **99** (1995) 11584.
- [188] JOHARI G. P., *J. Phys. Chem. B*, **102** (1998) 4711.
- [189] SMITH R. S. and KAY B. D., *Nature*, **398** (1999) 788.
- [190] McCLURE S. M., SAFARIK D. J., TRUSKETT T. M. and MULLINS C. B., *J. Phys. Chem. B*, **110** (2006) 11033.
- [191] ITO K., MOYNIHAN C. T. and ANGELL C. A., *Nature*, **398** (1999) 492.
- [192] LOERTING T., BRAZHUKIN V. V. and MORISHITA T., *Adv. Chem. Phys.*, **143** (2009) 29.
- [193] ANDERSSON O., *Proc. Natl. Acad. Sci. U.S.A.*, **108** (2011) 11013.
- [194] POOLE P. H., SCIORTINO F., ESSMANN U. and STANLEY H. E., *Nature*, **360** (1992) 324.
- [195] MISHIMA O. and STANLEY H. E., *Nature*, **392** (1998) 164.
- [196] MISHIMA O., *J. Chem. Phys.*, **115** (2001) 4199.
- [197] MISHIMA O., *J. Chem. Phys.*, **121** (2004) 3161.
- [198] ANDERSSON O., *Phys. Rev. Lett.*, **95** (2005) 205503.
- [199] ANDERSSON O. and INABA A., *Phys. Rev. B*, **74** (2006) 184201.
- [200] SEIDL M., ELSAESSER M. S., WINKEL K., ZIFFERER G., MAYER E. and LOERTING T., *Phys. Rev. B*, **83** (2011) 100201.
- [201] HANDLE P. H., SEIDL M. and LOERTING T., *Phys. Rev. Lett.*, **108** (2012) 225901.
- [202] AMANN-WINKEL K., GAINARU C., HANDLE P. H., SEIDL M., NELSON H., BOHMER R. and LOERTING T., *Proc. Natl. Acad. Sci. U.S.A.*, **110** (2013) 17720.
- [203] RUIZ G. N., BOVE L. E., CORTI H. R. and LOERTING T., *Phys. Chem. Chem. Phys.*, **16** (2014) 18553.